Bioactive Materials 10 (2022) 443–459

Contents lists available at ScienceDirect

Bioactive Materials

journal homepage: www.sciencedirect.com/journal/bioactive-materials

Tropoelastin improves adhesion and migration of intra-articular injected infrapatellar fat pad MSCs and reduces osteoarthritis progression☆

Junjun Yang [a], Xin Wang [a], Yahan Fan [c], Xiongbo Song [a], Jiangyi Wu [d], Zhenlan Fu [a], Tao Li [a], Yang Huang [a], ZheXiong Tang [a], Shuo Meng [b], Na Liu [a,e], Jiajia Chen [f], Pingju Liu [g], Liu Yang [a,*], Xiaoyuan Gong [a,**], Cheng Chen [b,***]

[a] Center for Joint Surgery, Southwest Hospital, Army Medical University (Third Military Medical University), Chongqing, 400038, China
[b] College of Medical Informatics, Chongqing Medical University, Chongqing, 400016, China
[c] Blood Transfusion Department, Southwest Hospital, Army Medical University (Third Military Medical University), Chongqing, 400038, China
[d] Department of Sports Medicine, Peking University Shenzhen Hospital, Peking University, Shenzhen, 518036, China
[e] Key Laboratory of Freshwater Fish Reproduction and Development, Ministry of Education, Laboratory of Molecular Developmental Biology, School of Life Sciences, Southwest University, Chongqing, 400038, China
[f] Biomedical Analysis Center, Army Medical University (Third Military Medical University), Chongqing, 400038, China
[g] Department of Orthopedics, Zunyi Traditional Chinese Medicine Hospital, Zunyi, 563099, China

ARTICLE INFO

Keywords:
Tropoelastin
Osteoarthritis
Infrapatellar fat pad MSCs

ABSTRACT

Intra-articular injection of mesenchymal stem cells (MSCs) is a promising strategy for osteoarthritis (OA) treatment. However, more and more studies reveal that the injected MSCs have poor adhesion, migration, and survival in the joint cavity. A recent study shows that tropoelastin (TE) regulates adhesion, proliferation and phenotypic maintenance of MSCs as a soluble additive, indicating that TE could promote MSCs-homing in regenerative medicine. In this study, we used TE as injection medium, and compared it with classic media in MSCs intra-articular injection such as normal saline (NS), hyaluronic acid (HA), and platelet-rich plasma (PRP). We found that TE could effectively improve adhesion, migration, chondrogenic differentiation of infrapatellar fat pad MSCs (IPFP-MSCs) and enhance matrix synthesis of osteoarthritic chondrocytes (OACs) in indirect-coculture system. Moreover, TE could significantly enhance IPFP-MSCs adhesion via activation of integrin β1, ERK1/2 and vinculin (VCL) *in vitro*. In addition, intra-articular injection of TE-IPFP MSCs suspension resulted in a short-term increase in survival rate of IPFP-MSCs and better histology scores of rat joint tissues. Inhibition of integrin β1 or ERK1/2 attenuated the protective effect of TE-IPFP MSCs suspension *in vivo*. In conclusion, TE promotes performance of IPFP-MSCs and protects knee cartilage from damage in OA through enhancement of cell adhesion and activation of integrin β1/ERK/VCL pathway. Our findings may provide new insights in MSCs intra-articular injection for OA treatment.

1. Introduction

Osteoarthritis (OA) is a chronic, multicausal, and progressive joint disease characterized by degeneration of the articular cartilage and remodeling of other joint tissues [1]. With the development of tissue engineering, mesenchymal stem cells (MSCs)-based therapies for OA have been widely studied and used in clinics [2]. For knee OA treatment, intra-articular injection of MSCs, including bone marrow-derived stem cells (BMSCs) and adipose-derived stem cells (ADSCs), has been proven to be a safe therapy [3]. Studies have shown that intra-articular injection of BMSCs is effective in improving joint function and decreasing knee OA symptoms [4,5]; injection of ADSCs also improves VAS and KOOS-sports/recreation in OA patients [6]. Moreover, MSCs therapies could preserve articular cartilage superficial layer cells, inhibit synovitis

☆ The first two authors (Junjun Yang and Xin Wang) contributed equally to this paper.Peer review under responsibility of KeAi Communications Co., Ltd.

* Corresponding author.
** Corresponding author.
*** Corresponding author.
E-mail addresses: jointsurgery@163.com (L. Yang), sliegxy@gmail.com (X. Gong), ccljjff@163.com (C. Chen).

https://doi.org/10.1016/j.bioactmat.2021.09.011
Received 15 June 2021; Received in revised form 7 September 2021; Accepted 7 September 2021
Available online 15 September 2021

[7], and relieve vascular infiltration of subchondral bone [8]. However, a recent systematic review reports that MSCs injection is not superior to placebo in pain relief and functional improvement for patients with symptomatic knee OA [9]. For instance, MSCs could move towards and accumulate around impaired cartilage but not have significant therapeutic effect on OA [10]; the galectin expression and motility of BMSCs are impaired after intra-articular injection, which limits tissue repair in OA [11]; MRI results show that MSCs do not participate in repair of cartilage defects following intra-articular injection [12]. In addition, many factors, such as no uniform standard for clinical use [13], unclear mechanism of OA treatment after MSCs injection [14], and microenvironment of injection site [15] have led to restrictions on application of MSCs. Therefore, the performance of the injected MSCs in OA joints needs further study.

Due to the complex biomechanical microenvironment in joint, the MSCs lack effective adhesion to the extracellular matrix (ECM) after injection [16]. It has been shown that few survived MSCs are tracked in knee joint at 7 days or 14 days after injection [17,18]; only a small part of MSCs could adhere to cartilage or synovium after intra-articular injection [19,20]; MSCs are no longer detectable 3 weeks after intra-articular injection although it has beneficial effects on treatment of OA [21,22]. Because the adhesion and long-term survival of MSCs are prerequisites for cell therapy [23], improving adhesion and homing of MSCs in the joint cavity might improve the curative effect of intra-articular injection therapies for OA treatment.

Tropoelastin (TE) is the dominant building block of elastic fibers, providing structural support to tissues and imbuing them with elasticity and resilience [24]. TE has been shown to promote sequential cell attachment and spreading [25,26]. More importantly, a recent study suggests that TE could regulate adhesion, proliferation, and phenotypic maintenance of MSCs as a soluble additive [27]. Hence, we assumed that TE might be used to improve the performance of injected MSCs in OA joints. Firstly, we investigated the effect of TE on adhesion, migration, chondrogenic differentiation, and paracrine function of infrapatellar fat pad MSCs (IPFP-MSCs) *in vitro*. Then, the intra-articular performance of IPFP-MSCs and therapeutic effect of TE-IPFP-MSCs suspension injection on OA were observed in rat knee OA model. The underlying mechanism of TE regulating IPFP-MSCs performance was also analyzed. Normal saline (NS) [28], hyaluronic acid (HA) [29], and platelet-rich plasma (PRP) [30], the classic media of MSCs injection in clinics, were used as control.

2. Materials and methods

2.1. Ethics, inclusion criteria and exclusion criteria

This study was approved by the Ethics Committee of Southwest Hospital, Chongqing, China. All patients involved in this study had signed the informed consent form. Only patients with advanced knee OA (grade IV in The Kellgren-Lawrence grading system) were selected, and patients with inflammatory arthritis or with a history of prior knee surgery were excluded.

2.2. Isolation, culture, and identification of primary human IPFP-MSCs

Infrapatellar fat pad (IPFP) samples were obtained from OA patients (three male and three female, average age 59.33 ± 3.01 years) undergoing total knee arthroplasty as described previously [31]. Small pieces of IPFP were washed in PBS (Beyotime) and digested with 0.2% collagenase I (Sigma) in DMEM/F12 (Gibco) supplemented with 1% P/S (Beyotime) at 37 °C + 5% CO_2 overnight. The digested cell suspension was filtered through a 100-μm and 40-μm cell strainer (Millipore). The resulting cell suspension was centrifuged at 500 g for 5 min. The supernatant was removed, and red blood cell lysis buffer (Beyotime) was added. Cells were centrifuged again (500 g for 5 min) and resuspended in DMEM/F12 supplemented with 10% FBS (Gibco) and 1% P/S. The medium was changed every 2 days. Cells were used at passage 3 to avoid phenotype changes of IPFP-MSCs.

To identify IPFP-MSCs, Human MSCs Analysis Kit (BD Biosciences) was utilized to test antigens including positive markers CD44, CD73, CD90, and CD105 and negative markers CD11b, CD19, CD34, CD45, and HLA-DR following the manufacturer's instructions. Besides, immunofluorescence staining was performed to detect expression of positive markers in IPFP-MSC including CD44, CD90, and CD105.

2.3. Isolation, culture, and identification of primary human osteoarthritic chondrocytes (OACs)

Cartilage samples (donor-matched) were obtained from OA patients (three male and three female, average age 59.33 ± 3.01 years) undergoing total knee arthroplasty as described previously. Cartilage fragments were washed in PBS and digested with 0.2% collagenase II (Sigma) in DMEM/High glucose medium (Gibco) supplemented with 1% P/S at 37 °C + 5% CO_2 overnight. The digested cell suspension was filtered through a 40-μm cell strainer. After being centrifuged (400 g for 5 min), chondrocytes were resuspended in DMEM/High glucose medium supplemented with 10% FBS and 1% P/S. Cells were used at passage 1 to avoid phenotype changes of OACs. HE staining (Sigma) and Safranin O staining (Solarbio) were carried out to observe OACs morphology and glycosaminoglycans (GAGs) expression.

2.4. Cell labeling

In order to track IPFP-MSCs on surface of human cartilage or in rat knee articular cavity, IPFP-MSCs were incubated with DiO (Beyotime) or DiI (Beyotime) or DiR (ThermoFisher) (10 μM). Briefly, stock solution of DiO or DiI or DiR was dissolved in DMSO (Gibco) (10 mM), and diluted in DMEM/F12. Labeled IPFP-MSCs were observed by Inverted fluorescence microscope (IX71 Olympus).

2.5. Isolation of human knee osteochondral composites

The knee articular cartilages were obtained from OA patients (three male and three female, average age 59.83 ± 2.48 years). For isolation of human knee osteochondral composites, hollow medical electrical trepan-drill was used. The drill was perpendicular to surface of cartilage. The isolated osteochondral samples were used in following experiments.

2.6. Experimental preparation and design

NS (0.9% NaCl; Sichuan Kelun Pharmaceutical) and HA (ARTZ® Dispo; Kunming Baker Norton Pharmaceutical; Imported Drug License: H20140533) were within the expiration date. PRP (Blood Transfusion Department of Southwest Hospital) was separated and concentrated from the whole blood of health adults (three male and three female, average age 26.33 ± 2.16 years; platelet concentration: ~1300 × 10^9/L). TE (Advanced BioMatrix) was dissolved in 0.25% glacial acetic acid (Beyotime) and diluted with NS to reach the concentration of 20 μg/mL. The pH value was 6.76 for NS, 7.32 for HA, 6.83 for PRP, and 6.61 for TE. Considering the lack of nutrient in NS, HA, and TE for long-term IPFP-MSCs survival, equal proportion of medium (DMEM/F12 or chondrogenic differentiation medium) was added to these solvents during cell culture *in vitro*.

2.7. IPFP-MSCs adhesion to cell slide or on human knee cartilage surface

IPFP-MSCs (5 × 10^4 cells) suspended in NS or HA or PRP or TE + DMEM/F12 solution (mixing ratio: 1:1) were seeded into cell slide (24-well plates) and incubated for 2 h [27] at 37 °C, then washed with divalent cation-free PBS solution (Sigma) to remove the non-adherent cells. The attached cells were fixed in 4% paraformaldehyde (Beyotime), stained with crystal violet (Beyotime) for 1 h, and counted with

Image-Pro Plus 6.0 (Media Cybernetics). For scanning electron microscope (SEM) scanning, the IPFP-MSCs on cell-slide were fixed (glutaraldehyde), dehydrated (ethyl alcohol and tertiary butanol) and sputter-coated with gold. The morphologies of cells were viewed with a Crossbeam 340 SEM (ZEISS) operated at 2 kV accelerating voltage, and the area of adherent cells was calculated with bundled software. For Pro-film 3D scanning, cells were fixed with 4% paraformaldehyde and cell height was detected with ProfilmOnline (Filmetrics).

Human knee osteochondral samples were trimmed for cylindrical shape and then placed into 48-well plates. To mimic attachment process of IPFP-MSCs to cartilage, DiI-IPFP-MSCs suspension was added onto surface of cartilage dropwise. Thereafter, 48-well plates were put into incubator at 37 °C + 5% CO_2 for 6 h [32]. Cartilage surface was gently washed by divalent cation-free PBS solution. Confocal microscopy was used to image attached cells: (1) Cartilage was placed directly in a confocal dish and DiI-IPFP-MSCs located on surface of cartilage were scanned; (2) Cartilage was fixed in 4% paraformaldehyde and stained by DAPI solution. Nuclei of DiI-IPFP-MSCs attached to cartilage surface were scanned. (3) Cartilage fixed with 4% paraformaldehyde. Cells on outmost surface of cartilage were scanned.

2.8. Scratch test and transwell migration assay

IPFP-MSCs were seeded into Culture-Insert 2 Well in μ-Dish ^{35mm} (Ibidi) or onto cartilage surface, and cultured for 24 h. Culture-Insert was removed and scratches on cartilage were made in the plate using a P200 pipette tip. After washing with PBS three times, the culture medium was changed with DMEM/F12 supplemented with 0.9% NS or HA or PRP or TE (mixing ratio: 1:1). To analyze the migration of IPFP-MSCs, images were taken at 0, 24, and 48 h, and cells that crossed the baseline were counted for analysis.

Besides, 5×10^4 cells/well of IPFP-MSCs were seeded into the upper chamber of Transwell (Corning, 8 μm) filled with DMEM/F12. The lower chamber was filled with DMEM/F12 supplemented with 0.9% NS or HA or PRP or TE (mixing ratio: 1:1). After 24 h, cells in the upper surface of the membrane were removed with a cotton swab. Cells that migrated to the other side of the membrane were fixed with 4% paraformaldehyde and stained with crystal violet. These cells were imaged and counted in 6 random view fields.

2.9. Mechanism of IPFP-MSCs adhesion in vitro

To further clarify the mechanism of adhesion, IPFP-MSCs (5×10^4 cells) were seeded into cell-slides and incubated for 2 h or 6 h or 12 h at 37 °C. Expression of VCL and cytoskeleton was detected by Laser scanning confocal microscope (LSM780 ZEISS). Besides, expression of genes associated with adhesion including integrin linked kinase (ILK), contactin 4 (CNTN4), fibronectin 1 (FN1), elastin (ELN), laminin subunit alpha 5 (LAMA-5), microfibril associated protein 4 (MFAP4), nidogen 2 (NID2), thrombospondin 1 (THBS1), vimentin (VIM), vitronectin (VTN), dermatopontin (DPT), VCL, periostin (POSTN), extracellular regulated protein kinases (ERK), protein tyrosine kinase 2 (PTK2), and high mobility group box 1 (HMGB1) was analyzed when IPFP-MSCs were attached for 6 h. Moreover, integrin subunit alpha 1–5 (integrin α1, α2, α3, α4, α5) and integrin subunit beta 1–5 (integrin β1, β2, β3, β4, β5) were also measured.

IPFP-MSCs (5×10^4 cells) were seeded into cell-slides filled with TE-DMEM/F12 solution (mixing ratio: 1:1) containing 5 mM EDTA [27] (Biosharp). The cells were incubated for 2 h at 37 °C, then washed with cation-free PBS to remove non-adherent cells. The attached cells were fixed and stained, and cell attachment was quantified. To block specific integrin (integrin β1) or ERK1/2 activity, IPFP-MSCs were pretreated with 10 μg/mL of anti-integrin β1 [33–35] (Abcam) or 5 nM EAK1/2 inhibitor SCH772984 [36,37] (TOPSCIENCE) for 12 h, washed with divalent cation-free PBS to removed antibodies or inhibitor and then suspended in TE solution. TE-coated model was also established by adding TE solution to cell-slide, incubated at 37 °C for 2 h, and then washed with double distilled water before cell attachment. The nonspecific mouse IgG (10 μg/mL) (Sigma) was included as a negative control for anti-integrin β1.

2.10. Chondrogenic potential of IPFP-MSCs and its effect on phenotype of OACs in co-culture

IPFP-MSCs (5×10^4 cells) were seeded into cell-slide or onto cartilage surface and grew until 100% confluence. Cells were maintained at 37 °C + 5% CO_2 incubator, and the induction medium (NS or HA or PRP or TE + chondrogenic differentiation medium, mixing ratio: 1:1) (CYAGEN) was replaced every 2 days. After 7 days of culture in induction medium, expression of collagen II, aggrecan, and SOX-9 was measured in IPFP-MSCs. IPFP-MSCs at passage 3 and OACs at passage 1 from a single patient were used in coculture. For indirect-coculture, OACs were seeded into the lower chamber of Transwell filled with DMEM/F12; IPFP-MSCs were seeded into the upper chamber of Transwell (Corning, 0.4 μm) filled with DMEM/F12 supplemented with 0.9% NS or HA or PRP or TE (mixing ratio: 1:1); OACs alone were used as control. After 7 days of coculture, expression of collagen II, aggrecan, and SOX-9 was detected in OACs.

2.11. Immunofluorescence staining

IPFP-MSCs or OACs were fixed in 4% paraformaldehyde. Nonspecific bindings were blocked with QuickBlock blocking buffer (Beyotime) for 2 h. Fixed cells were incubated with primary antibodies (collagen II, aggrecan, SOX-9, VCL, integrin β1, ERK1/2 and p-ERK1/2) (Abcam) overnight at 4 °C, followed by incubation with secondary antibody (Ms-647 or Rb-488) (Abcam) for 90 min at room temperature. Nuclei were stained with DAPI (Beyotime) for 8 min. Samples were observed by Laser scanning confocal microscope (LSM780 ZEISS). The relative fluorescence unit (RFU) was analyzed using ZEN 2012 software. Three different fluorescence images among each group were used for statistical analysis (total fluorescence intensity of the image/number of nuclei).

2.12. Western blot analysis

Total protein was extracted from the IPFP-MSCs using RIPA lysis buffer (Beyotime) supplemented with protease-phosphatase inhibitors (Roche) on ice for 20 min, followed by centrifugation at 12,000*g* for 30 min at 4 °C. Protein concentration was determined using BCA protein assay kit (Beyotime). Next, 50 ng of protein was separated by SDS PAGE (Beyotime) and subsequently transferred to PVDF membrane (Millipore). The membranes were blocked with QuickBlock blocking buffer overnight at 4 °C and then incubated overnight at 4 °C with the primary antibodies (collagen II, aggrecan, SOX-9, VCL, integrin β1, ERK1/2 and p-ERK1/2), followed by incubation with respective secondary antibodies for 1 h at room temperature. After washing three times with TBST, the membranes were visualized using SuperSignal west femto kit (ThermoFisher). Finally, the intensity of the blots was quantified with Image Lab 3.0 software (Bio-Rad).

2.13. Quantitative RT-PCR analysis

As for mRNA detection, the IPFP-MSCs were lysed and total RNA was extracted using TRIzol reagent. Complementary DNA templates were generated by using Transcriptor first strand cDNA synthesis kit (Roche). RT-PCR was performed on Bio-Rad CFX96-Touch system by using FastStart essential DNA green master (Roche), with each sample prepared in triplicate according to the manufacturer's recommendation. β-actin was used as the internal reference. The relative expression level of the mRNAs was calculated using the $2^{-\Delta\Delta CT}$ method.

2.14. Induction of rat knee OA

All animal experiments were in accordance to the animal research committee regulations of Third Military Medical University (Army Medical University). OA was induced in SD rats by anterior cruciate ligament transection (ACLT) as previously described [38]. Rats were anesthetized with 1% pentobarbital sodium, and the knee joint was exposed through a medial parapatellar approach. The patella was dislocated laterally, and the knee was placed in full flexion followed by ACLT with micro-scissors. Four weeks after OA induction, the rats received intra-articular injection of MSCs suspension.

2.15. Intra-articular injection of rat knee

In IPFP-MSCs tracking experiment, SD rats undergoing ACLT surgery were randomly divided into four groups: (1) NS-IPFP-MSCs suspension group; (2) HA-IPFP-MSCs suspension group; (3) PRP-IPFP-MSCs suspension group; (4) TE-IPFP-MSCs suspension group. There were 6 rats in each group. The rats were given intra-articular injections of 100 μL NS or HA or PRP or TE containing 3×10^5 fluorescently labeled IPFP-MSCs (only one injection).

To determine the effect of IPFP-MSCs intra-articular injection therapy, SD rats were randomly divided into six groups: (1) Control group; (2) ACLT group; (3) ACLT + 0.9% NS-IPFP-MSCs suspension; (4) ACLT + HA-IPFP-MSCs suspension; (5) ACLT + PRP-IPFP-MSCs suspension; (6) ACLT + TE-IPFP-MSCs suspension. There were 8 rats in each group. SD rats were given intra-articular injections of 100 μL NS or HA or PRP or TE containing 3×10^5 IPFP-MSCs with 1 mL syringe for 5 weeks (once a week).

To explore mechanism of IPFP-MSCs adhesion *in vivo*, SD rats were randomly divided into six group: (1) TE group; (2) TE + anti-integrin β1 pretreated IPFP-MSCs suspension; (3) anti-integrin β1 pretreated IPFP-MSCs suspension; (4) TE + IgG pretreated IPFP-MSCs suspension; (5) TE + SCH772984 pretreated IPFP-MSCs suspension; (6) SCH772984 pretreated IPFP-MSCs suspension. There were 6 rats in each group for *in vivo* imaging (only one injection), and there were 8 rats in each group for histology analysis (injected once a week for 5 weeks).

2.16. Distribution of IPFP-MSCs in rat knee articular cavity (confocal microscopy scanning)

After intra-articular injection with labeled IPFP-MSCs (only one injection), SD rats were sacrificed at 1 days, 3 days, 7 days, and 14 days. The femoral condyle, tibial plateau, and synovium were dissected out and placed in confocal dish. IPFP-MSCs attached to surface of these structures were analyzed by Laser scanning confocal microscope (LSM780 ZEISS).

2.17. Near-infrared fluorescence in vivo imaging

The SD rats undergoing ACLT surgery were divided into four groups: (1) NS-IPFP-MSCs suspension group; (2) HA-IPFP-MSCs suspension group; (3) PRP-IPFP-MSCs suspension group; (4) TE-IPFP-MSCs suspension group. SD rats were given intra-articular injections of 100 μL NS or HA or PRP or TE containing 3×10^5 DiR labeled IPFP-MSCs. Anesthesia of SD rats was induced by an intraperitoneal injection of pentobarbital sodium. After anesthesia, the skin around knee-joint was depilated, and the rats were placed into the *in vivo* imaging system. *In vivo* NIR fluorescence imaging was performed at 2 h, 1 days, 3 days, 7 days, and 14 days after injection. SD rats were sacrificed after fluorescent scanning of whole knee area. The femoral condyle, tibial plateau, meniscus, and synovium were dissected out and analyzed in the NIR fluorescence imaging system. The fluorescence intensities were analyzed using Living-image software. The color scale was 1e5 to 1e6 (Min to Max) and calculation-formula was $(p/sec/cm^2/sr)/(\mu W/cm^2)$.

2.18. Gross and histologic evaluation

The degree of cartilage regeneration was evaluated via gross examination. Representative sections of each sample were independently scored by 5 blinded observers according to the modified International Cartilage Repair Society (ICRS) gross grading scale.

For histologic analysis, rats were sacrificed, and knee joints were fixed in 4% paraformaldehyde, decalcified in 10% EDTA, and embedded in paraffin. Serial sagittal sections were obtained including the entire joint by collecting 5-μm sections at 50-μm intervals. Paraffin sections were subjected to HE staining, safranin O-fast green staining, and immunohistochemical staining of collagen II. Histologic changes in the rat knee joints were scored according to the recommendations of the Osteoarthritis Research Society International (OARSI) scoring system [39]. OARSI scoring system is sufficiently sensitive to discriminate between treatments and has high reproducibility, therefore it is recommended for evaluation of different OA models and treatments. The relative staining intensity of collagen II and GAGs in three central regions of articular cartilage was analyzed using Image-Pro Plus version 6.0 software.

2.19. Mechanism of IPFP-MSCs adhesion in vivo

IPFP-MSCs were pretreated with anti-integrin β1 or SCH772984 for 12 h, washed with divalent cation-free PBS and then suspended in TE solution. The IPFP-MSCs suspension was injected into SD rat's articular cavity. Survival of IPFP-MSCs was detected by *in vivo* NIR fluorescence imaging. The pathological changes of rat knee joint were revealed by histological evaluation.

2.20. Statistical analysis

Data were expressed as mean ± SD by using GraphPad prism 8.0 software. All *in vitro* experiments were repeated three times. Two different groups were compared by independent-sample *t*-test, and multiple group comparisons were performed by one way ANOVA with Tukey's post hoc test. The statistical significance among multiple ranked data was analyzed by Kruskal-Wallis test and Nemenyi test. In all cases, results were considered statistically significant when $P < 0.05$.

3. Results

3.1. Isolation, identification and labeling of IPFP-MSCs

Firstly, human infrapatellar fat pads were obtained from OA patients, and IPFP-MSCs were isolated according to the methods described in our pervious study [40] (Fig. S1A). We observed that IPFP-MSCs displayed a spindle morphology typical of MSCs. MSC markers were measured by using Flow Cytometry. Results showed that these cells were positive for the surface markers CD44 (98.63%), CD90 (99.72%), CD105 (98.56%), and CD73 (99.48%), negative for CD45, CD34, CD11b, CD19, and HLA-DR (1.14%) (Fig. S1B). Isolated cells conformed to identification of human MSCs proposed by the International Society for Cellular Therapy [41]. Immunofluorescence staining results also indicated that expression of CD44, CD90, and CD105 in these cells was detected at high levels (Fig. S1C). In addition, IPFP-MSCs were labeled with DiO or DiI or DiR for subsequent tracking experiment (Fig. S1D).

3.2. Isolation and identification of OACs

Firstly, human cartilage tissues were obtained from OA patients, and OACs were isolated according to the methods described in our previous study [42]. The cells displayed typical OACs morphology with paving-stone-like shape. Moreover, alcian blue staining and safranine O staining revealed that the isolated cells highly expressed GAGs (Fig. S1E).

3.3. TE in solution promotes IPFP-MSCs adhesion in vitro compared with NS, HA, and PRP

IPFP-MSCs were resuspended in the NS, HA, PRP, and TE + DMEM/F12 solution (1:1) and seeded (Fig. S1F). IPFP-MSCs were observed under optical microscope. Fig. S1G showed that cells in NS and TE group displayed small elliptic or round shape; cells in HA group showed three-dimensional multilayer cell-distribution due to viscoelasticity of HA; cells in PRP group were also in small elliptic or round shape but could not be seen clearly owing to suspended platelet. Cell slides were washed with divalent cation-free PBS, and the adherent cells were counted. Inverted microscope and crystal violet analysis (Fig. S1H) revealed that there were more remaining cells in TE group than that in NS, HA, and PRP group.

To further determine regulatory effect of NS, HA, PRP, and TE on cell adhesion, SEM and Pro-film 3D scanning were performed. As shown in Fig. 1A and D, IPFP-MSCs attached to cell-slide in TE group were more than those in NS, HA, and PRP group. In addition, the relative ratio of IPFP-MSCs with contact-adhesion-area greater than 1200 μm^2 in TE group was higher than NS, HA, and PRP group. Results of Pro-film 3D

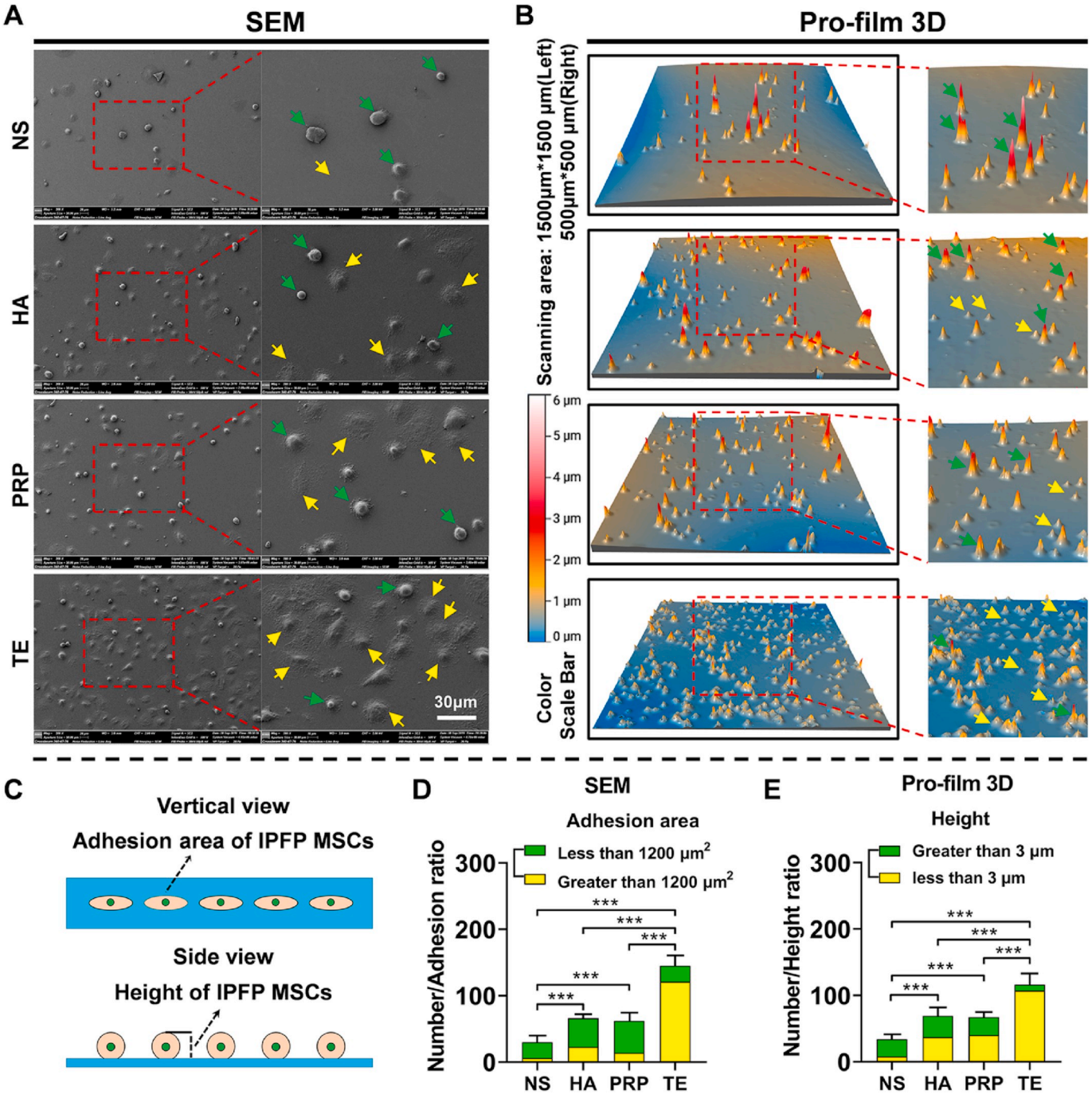

Fig. 1. TE regulates adhesion area and height of IPFP-MSCs in the early stage of adhesion to cell sides. (A) Morphology and adhesion area of IPFP-MSC observed by scanning electron microscope (SEM). Yellow arrows indicate IPFP-MSCs with adhesion area greater than 1200 μm^2; green arrows indicate IPFP-MSCs with adhesion area less than 1200 μm^2. (B) Height of IPFP-MSCs detected by Pro-film 3D. Yellow arrows indicate IPFP-MSCs with height less than 3 μm; green arrows indicate IPFP-MSCs with height greater than 3 μm. (C) Schematic diagram of adhesion area and height of IPFP-MSCs. (D) and (E) Quantitative analysis of number, adhesion area, and height of IPFP-MSCs. (n = 5, ***P < 0.001).

scanning also showed the same trend that IPFP-MSCs attached to cell-slide in TE group were more than those in NS, HA, and PRP group (Fig. 1B and E). Furthermore, in terms of cell height, the relative ratio of IPFP-MSCs with cell height less than 3 μm in TE group was higher than NS group, HA group, and PRP group. Brief schematic diagram of contact-adhesion-area and height was shown in Fig. 1C.

To mimic the process of IPFP-MSCs adhesion to cartilage *in vivo*, human knee osteochondral composites were obtained from surgical specimens and their shapes and sizes were shown in Fig. 2A. According to our experimental design (Fig. 2B), confocal 3D scanning results indicated that an almost confluent layer of IPFP-MSCs could be seen in TE group. DiI-IPFP-MSCs attached to cartilage surface in TE group were more than NS, HA, and PRP group. (Fig. 2C and F). In addition, number of DAPI-positive IPFP-MSCs nuclei on cartilage surface in NS group, HA group, and PRP group was less than that in TE group. (Fig. 2D and F). Besides, confocal light-microscope surface-scanning results showed similar trend (Fig. 2E and F).

3.4. TE promotes IPFP-MSCs migration in vitro compared with NS, HA, and PRP

The effect of NS, HA, PRP, and TE on migration of IPFP-MSCs was

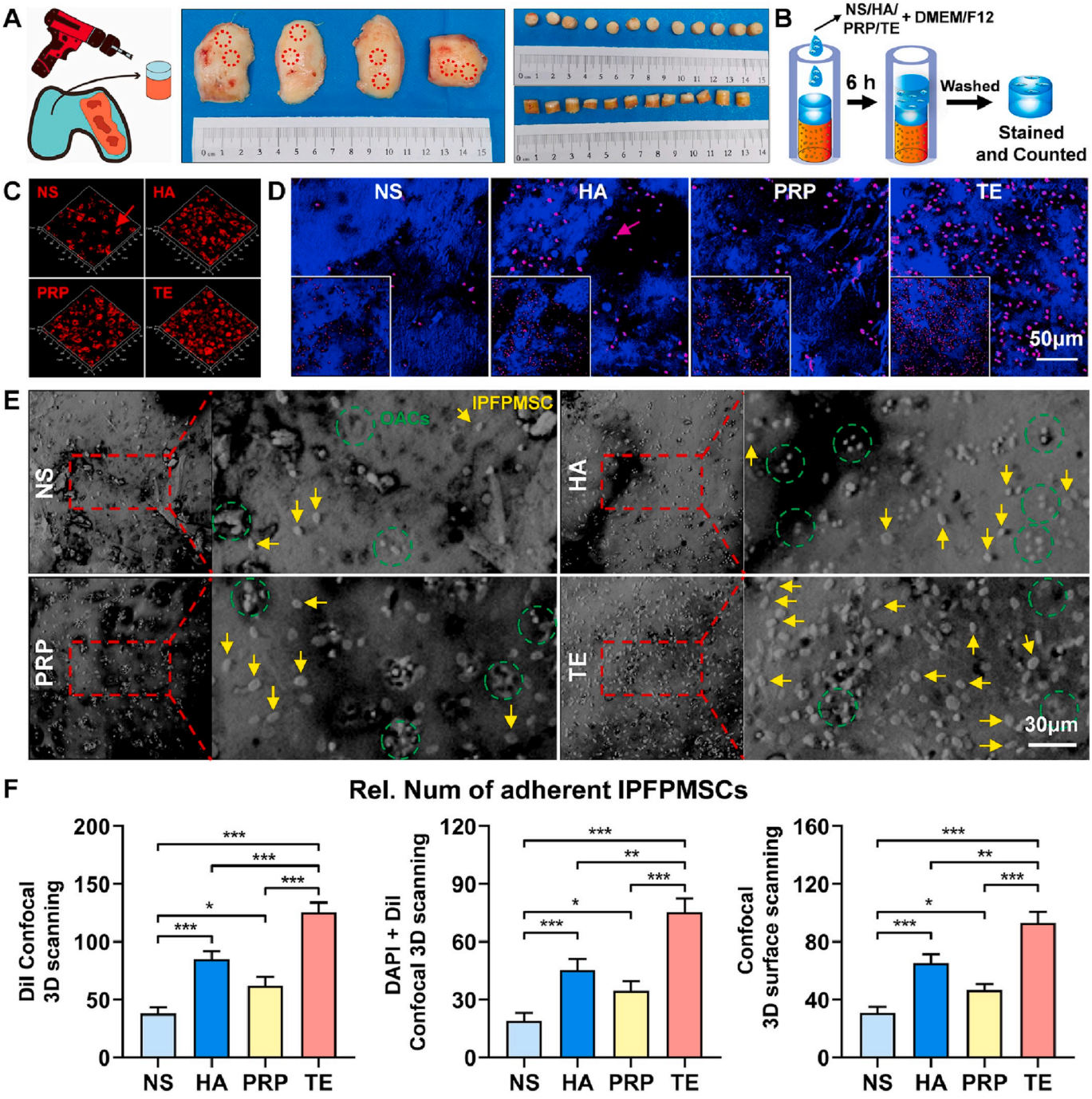

Fig. 2. TE improves adhesion of IPFP-MSCs on human knee osteochondral composites (hOCCs). (A) Isolation of hOCCs and its size-shape. (B) Flowchart exemplifying IPFP-MSCs-OCCs adhesion experiment procedure. (C) and (D) DiI-IPFP-MSCs attached to hOCCs. Red arrows and purple arrows (red mixed with blue) indicate DiI-IPFP-MSCs. (E) Confocal 3D surface scanning of hOCCs. Yellow arrows indicate IPFP-MSCs; green circles show OACs in cartilage lacuna. (F) Quantitative analysis of IPFP-MSCs adhesion on cartilage. (n = 3, *P < 0.05, **P < 0.01, ***P < 0.001).

examined through scratch test and Transwell migration assay (Fig. S2A). In Culture-Insert 2 Well in μ-Dish or on cartilage surface, the number of migrated IPFP-MSCs in the NS, HA, and PRP group was less than that in TE group at 24 h or 48 h (Figs. S2D and S2E; Fig. 3A, B, 3C and 3D). Similarly, in Transwell migration assay, IPFP-MSCs that migrated from the upper membrane to the other side in TE group at NS, HA, and PRP group were more than those in NS, HA, and PRP group (Figs. S2B and S2C).

3.5. TE increases expression of chondrogenic markers in IPFP-MSCs and OACs

To evaluate potential of TE to repair cartilage damage, chondrogenic differentiation and paracrine activities of IPFP-MSCs in TE solution were measured (Fig. 3E). During chondrogenic differentiation of IPFP-MSCs, immunofluorescent staining results (Fig. 3F) showed that there was no significant difference in changes of cytoskeleton among four groups; IPFP-MSCs of NS and PRP group had fewer expressions in collagen II, aggrecan, and SOX-9 compared to HA and TE group. Besides, RFU statistical analysis results also showed that addition of TE and HA increased the expression of chondrogenic markers in IPFP-MSCs compared with NS and PRP (Fig. 3G). At protein levels (Fig. 3H), Western blot results also revealed that TE and HA increased expression of chondrogenic markers compared with NS and PRP. Similarly, IPFP-MSCs attached to the cartilage of TE and HA group had greater expression in collagen II (Fig. 3I). In addition, in the indirect co-culture system, fluorescent staining and its RFU analysis indicated a higher expression of collagen II, aggrecan, and SOX-9 in OACs of TE group and PRP group (Fig. 3J and K). Besides, at protein levels, TE and PRP increased expression of chondrogenic markers compared with NS and HA in OACs (Figure 3L).

3.6. TE modulates cytoskeleton and expression of VCL in IPFP-MSCs

In Fig. 4A, at 2 h, IPFP-MSCs in NS, HA, and PRP group were round with compact cytoskeleton, and a few dot-like focal complexes could be seen at cell periphery. In TE group, there were a number of dot-like focal complexes and streak-like focal adhesions at the IPFP-MSCs center and periphery; phalloidin staining showed that IPFP-MSCs were in polygonal shape with slightly loose cytoskeleton. Fluorescent statistical analysis (Fig. 4B) and western-blot (Fig. 4C and D) also revealed that TE significantly increased the expression of VCL compared with NS, HA, and PRP group in IPFP-MSCs; expression of VCL in HA and PRP group was higher than that in NS group. At 6 h, the distribution of cytoskeleton among four groups showed no significant difference. Expression of VCL in TE group was higher than that in NS, HA, and PRP group; HA and PRP group higher than NS group. At 12 h, immunofluorescent staining results showed that there was no significant difference in changes of cytoskeleton among four groups. Besides, expression of VCL demonstrated a trend of upregulation in the HA, PRP, and TE group compared with the NS group; no significant difference was noted in expression of VCL among HA, PRP, and TE group.

3.7. TE promotes IPFP-MSCs adhesion via integrin β1/ERK/VCL pathway

Inverted microscope and crystal violet results (Figs. S3A and S3B) showed that there were more adherent cells in TE group than in TE + EDTA group and EDTA group. In order to explore the underlying mechanism of IPFP-MSC adhesion, 16 adhesion related genes and 10 integrin subtype genes were tested. As shown in Fig. 5A and B, 12 genes were differentially expressed between TE group and NS group; 9 genes between PRP group and NS group; 7 genes between HA group and NS group. Among these differentially expressed genes, mRNAs containing VCL, ERK, and integrin β1 were dramatically increased in TE-treated IPFP-MSCs. Furthermore, immunofluorescence analysis and Western blot results (Fig. 5C, D, and 5G) confirmed that TE manifestly increased the expression of integrin β1 and ERK 1/2.

Taken together the results above, we focused on the integrin β1/ERK/VCL signaling pathway to further investigate the mechanism of TE in regulating adhesion in IPFP-MSCs. The integrin β1 monoclonal antibody (anti-integrin β1) and ERK1/2 inhibitor (SCH772984) were used (Fig. S3C). IgG was used as control. As shown in Figs. S3D, S3E, S3H, and S3I, the number of IPFP-MSCs in TE + anti-β1 group and anti-β1 group was significantly less than that in TE group and TE + IgG group. In addition, compared with TE group or TE + IgG group, integrin β1 monoclonal antibody markedly decreased expression of integrin β1, ERK1/2, and VCL in TE + anti-β1 group or anti-β1 group. When ERK 1/2 protein levels were used as relative internal reference, the activation ratio of p-ERK1/2 was also decreased in TE + anti-β1 group or anti-β1 group (Fig. 5E, F, and 5H). With addition of SCH772984, there were fewer adherent IPFP-MSCs in TE + SCH group and SCH group as compared with TE group (Figs. S3F and S3G). Similarly, it demonstrated that ERK1/2 inhibitor SCH772984 decreased expression of ERK1/2 and VCL in TE + SCH group and SCH group. Besides, at protein expression of p-ERK1/2, Western blot results showed similar trend (Fig. 5I–K).

3.8. TE promotes IPFP-MSCs survival and adhesion in rat joint cavity

Intra-articular-anoikis of MSCs is a key factor influencing curative effect of MSCs-based therapy [43], therefore, survival number of IPFP-MSCs and its distribution in joint cavity were measured. DiO or DiI labeled-IPFPMSCs were injected into rat knee joint according to our experimental design (Fig. 6A). The femoral condyle, tibial plateau, meniscus, and synovium were dissected out from rat knee joint (Fig. 6B), and IPFP-MSCs attached to them were scanned under confocal microscopy.

At 1 d or 3 d (Fig. 6C), IPFP-MSCs attached to femoral condyle or tibial plateau or synovium in TE and HA group were more than those in NS and PRP group, but there was no significant difference in number of cells attached to meniscus among four groups. At 7 d or 14 d (Fig. 6C), there was no significant difference in number of IPFP-MSCs adhering to these structures among four groups. Quantitative analysis of IPFP-MSCs adhesion on rat femoral condyle or tibia platform or synovium or meniscus also showed the same trend (Fig. 6D).

In addition, *in vivo* fluorescent imaging results and its semi-quantitative analysis (Fig. 6E and F) showed that fluorescence intensity of survived IPFP-MSCs in knee joint cavity in NS and PRP group was weaker than that in TE and HA group at 1 d or 3 d. However, at 7 d or 14 d, fluorescence intensity of knee joint in four groups was weak and fluorescence intensity among four groups showed no statistical difference. Besides, the femoral condyle, tibial plateau, meniscus, and synovium were dissected out from rat knee joint and their fluorescence intensities were also measured. Compared with NS and PRP, TE and HA solution increased fluorescence intensity of these tissues at 1 d or 3 d. However, there was no significant difference in fluorescence intensity among four groups at 7 d or 14 d.

3.9. Intra-articular injection of TE-IPFP-MSCs suspension effectively reduces rat knee OA

To evaluate the role of TE-IPFP-MSCs suspension on protection of articular cartilage, the ACLT-induced rat OA model was used. The ACLT-induced OA rats were treated with IPFP-MSCs resuspended in NS or HA or PRP or TE according to the strategy shown in Fig. 7A. The knees in each group were isolated for macroscopic observation (Fig. 7B). Cartilage on the femoral condyles in control group appeared macroscopically normal with a smooth surface, and no cartilage defects or osteophytes were observed. In the ACLT group, cartilage surface was uneven-rough and some osteophytes were formed in knee joint. In addition, gross image of femoral condyle showed that NS, HA, PRP, and TE group had a smoother articular surface than ACLT group. However, there was no significant difference in macroscopic appearance among four groups

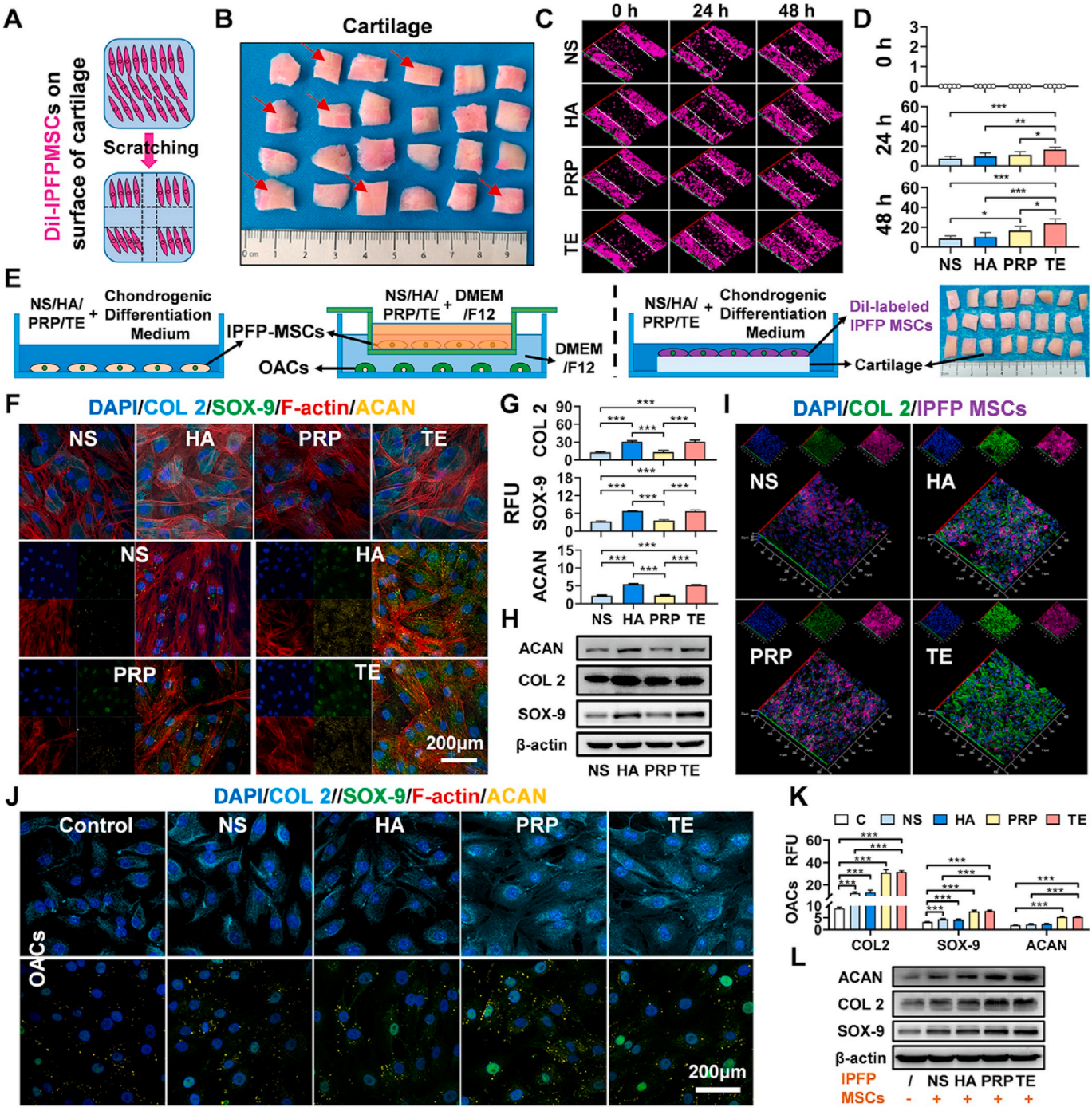

Fig. 3. TE enhances migration ability of IPFP-MSCs on cartilage surface, improves chondrogenic differentiation of IPFP-MSCs, and enhances matrix synthesis of OACs in indirect-coculture system. (A) and (B) Schematic diagram of scratch test performed on cartilage surface. Red arrows show scratch location. (C) Scratch test of IPFP-MSCs on cartilage surface. Confocal 3D scanning images were taken at 0, 24, and 48 h after scratching. White dashed lines indicate the baseline. (D) Quantification of IPFP-MSCs migrated across the baseline on cartilage surface. ($n = 5$, $^{*}P < 0.05$, $^{**}P < 0.01$, $^{***}P < 0.001$). (E) Schematic diagram of chondrogenic differentiation and indirect-coculture system. (F) Representative fluorescence images of F-actin (red), COL 2 (cyan), SOX-9 (green), and ACAN (yellow). Nuclei were stained with DAPI (blue). (G) The relative fluorescence unit (RFU) of COL 2, SOX-9, and ACAN was analyzed. ($n = 5$, $^{***}P < 0.001$). (H) Representative Western blot of COL 2, SOX-9, and ACAN. β-actin was served as a loading control for western blots (COL 2, SOX-9, and ACAN). (I) Representative confocal 3D scanning images of COL 2 (green). IPFP MSCs were labeled with DiI (purple). Nuclei were stained with DAPI (blue). (J) Representative fluorescence images of COL 2 (cyan), SOX-9 (green), and ACAN (yellow) in OACs. Nuclei were stained with DAPI (blue). (K) The relative fluorescence unit (RFU) of COL 2, SOX-9, and ACAN was analyzed (OACs). ($n = 5$, $^{***}P < 0.001$). (L) Representative Western blot of COL 2, SOX-9, and ACAN (OACs). β-actin was served as a loading control for western blots (COL 2, SOX-9, and ACAN).

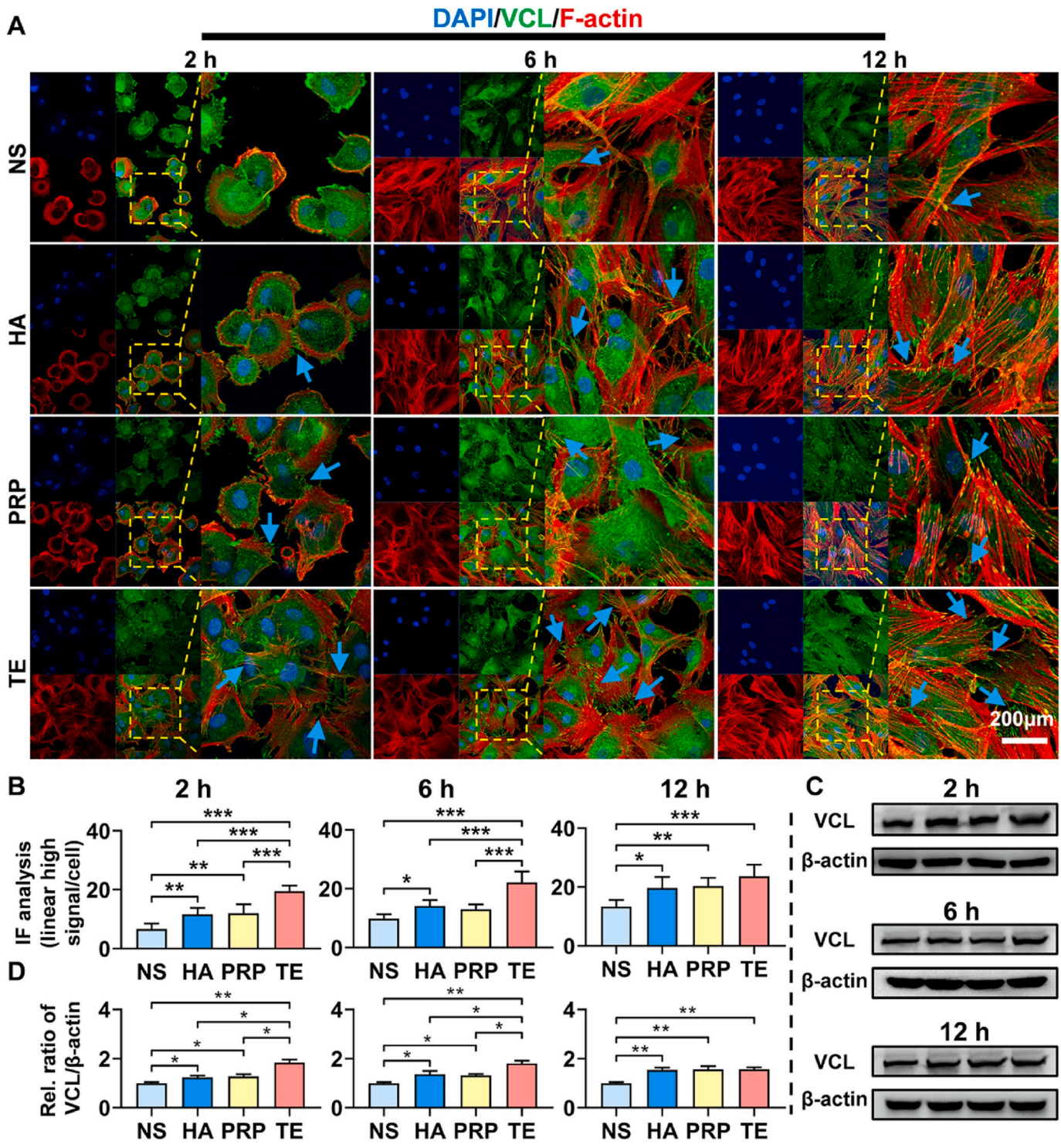

Fig. 4. TE promotes expression of VCL and cell spreading in IPFP-MSCs. (A) VCL immunofluorescence staining and morphology of the cytoskeleton in IPFP-MSCs at 2, 6, and 12 h after adherence. Blue arrows indicate intensive expression location of VCL. (B) Fluorescent quantitative analysis of VCL in IPFP-MSCs at 2, 6, and 12 h after adherence. (n = 5, *P < 0.05, **P < 0.01, ***P < 0.001). (C) and (D) Western blot of VCL and its statistical analysis (2, 6, and 12 h). (n = 3, *P < 0.05, **P < 0.01).

(NS, HA, PRP, and TE group) (Fig. 7C and E).

The damage of cartilage structure and proteoglycan loss were detected using HE and Safranin O/Fast Green staining. As the representative image shown in Fig. 7D, articular cartilage was obviously damaged after ACLT surgery. TE-treated rats knee joint showed complete integration of cartilage with a smooth surface, more expression of GAGs and regular arrangement of chondrocytes compared to the NS, HA and PRP injection group in ACLT-induced OA rats. Besides, the immunohistochemical experiment was carried out to assess the change of collagen II in articular cartilage of SD rat. The decreased expression of collagen II in cartilage was reversed by NS-IPFP-MSCs, HA-IPFP-MSCs, PRP-IPFP-MSCs, and TE-IPFP-MSCs suspension. In addition, compared with the ACLT group, the TE and HA group showed the best cartilage matrix deposition, followed by the PRP group, with NS group at last.

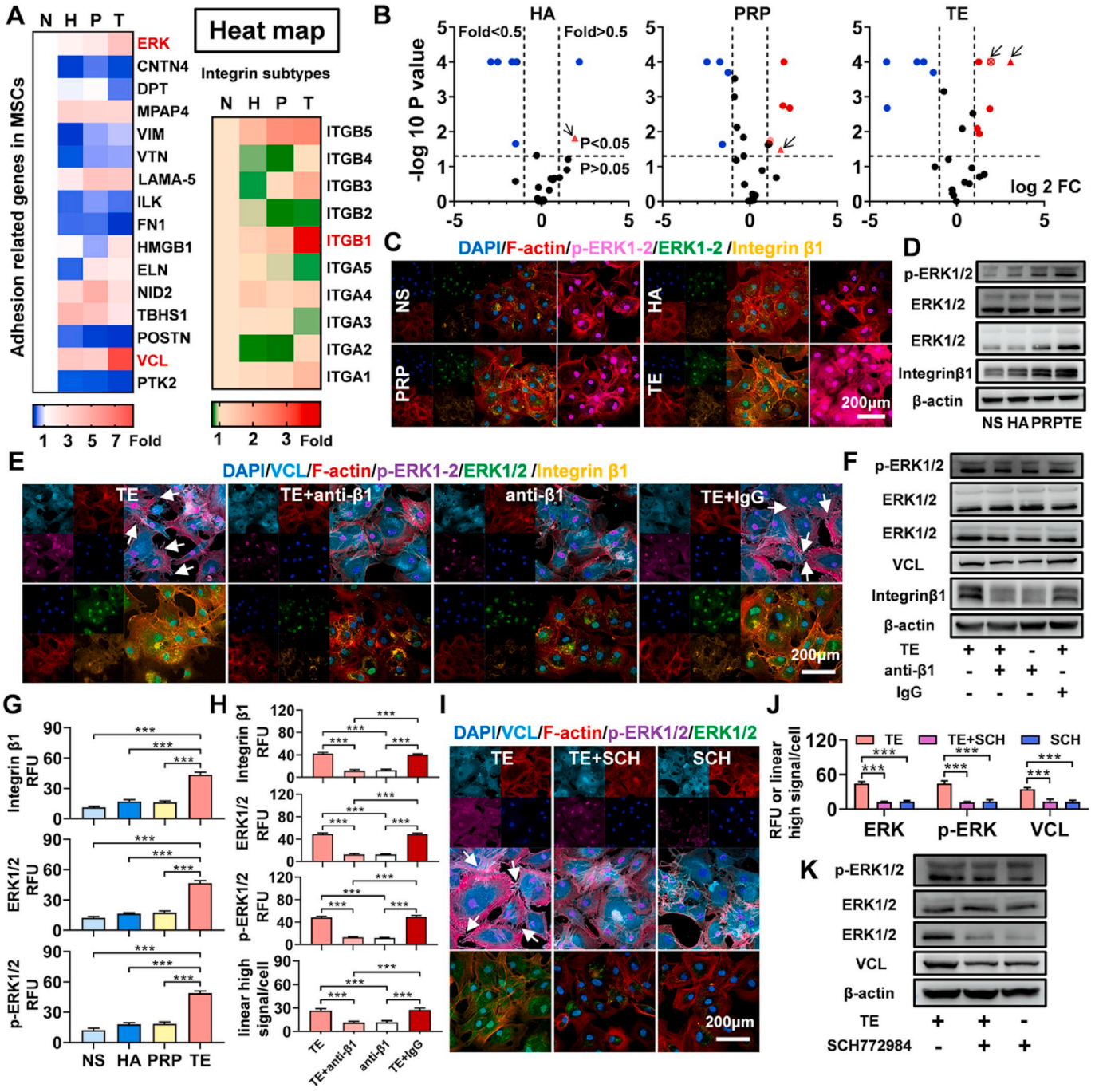

Fig. 5. TE promotes IPFP MSCs adhesion via integrinβ1/ERK/VCL pathway. (A) and (B) Heat map and volcano plots (16 adhesion related genes and 10 integrin subtype genes). Genes in red are related to TE regulating IPFP MSCs adhesion. The red triangles, circles, and rectangles represent VCL, ERK1/2, and integrin β1. (C) Representative immunofluorescence images of F-actin (red), integrin β1 (yellow), ERK1/2 (green) and p-ERK1/2 (purple). Nuclei were stained with DAPI (blue). (D) Representative Western blot of integrin β1 and ERK1/2. β-actin was served as a loading control for western blots (integrin β1 and ERK1/2). ERK1/2 was served as a loading control for western blots (activation ratio of p-ERK1/2). (E) Representative immunofluorescence images of F-actin (red), VCL (cyan), integrin β1 (yellow), ERK1/2 (green) and p-ERK1/2 (purple). Nuclei were stained with DAPI (blue). (F) Representative Western blot of integrin β1, VCL, and ERK1-2. β-actin was served as a loading control for western blots (integrin β1, vinculin, and ERK1/2). ERK1/2 was served as a loading control for western blots (activation ratio of p-ERK1/2). (G) The relative fluorescence unit (RFU) of integrin β1, ERK1/2, and p-ERK1/2 was analyzed. (n = 5, ***P < 0.001). (H) The relative fluorescence unit (RFU) of integrin β1, ERK1/2, and p-ERK1/2 and fluorescent quantitative analysis of VCL was analyzed. (n = 5, ***P < 0.001). (I) Representative immunofluorescence images of F-actin (red), VCL (cyan), ERK1/2 (green) and p-ERK1/2 (purple). Nuclei were stained with DAPI (blue). (J) The relative fluorescence unit (RFU) of ERK1/2 and p-ERK1/2 and fluorescent quantitative analysis of VCL was analyzed. (n = 5, ***P < 0.001). (K) Representative Western blot of vinculin and ERK1/2. β-actin was served as a loading control for western blots (VCL and ERK1/2). ERK1/2 was served as a loading control for western blots (activation ratio of p-ERK1/2).

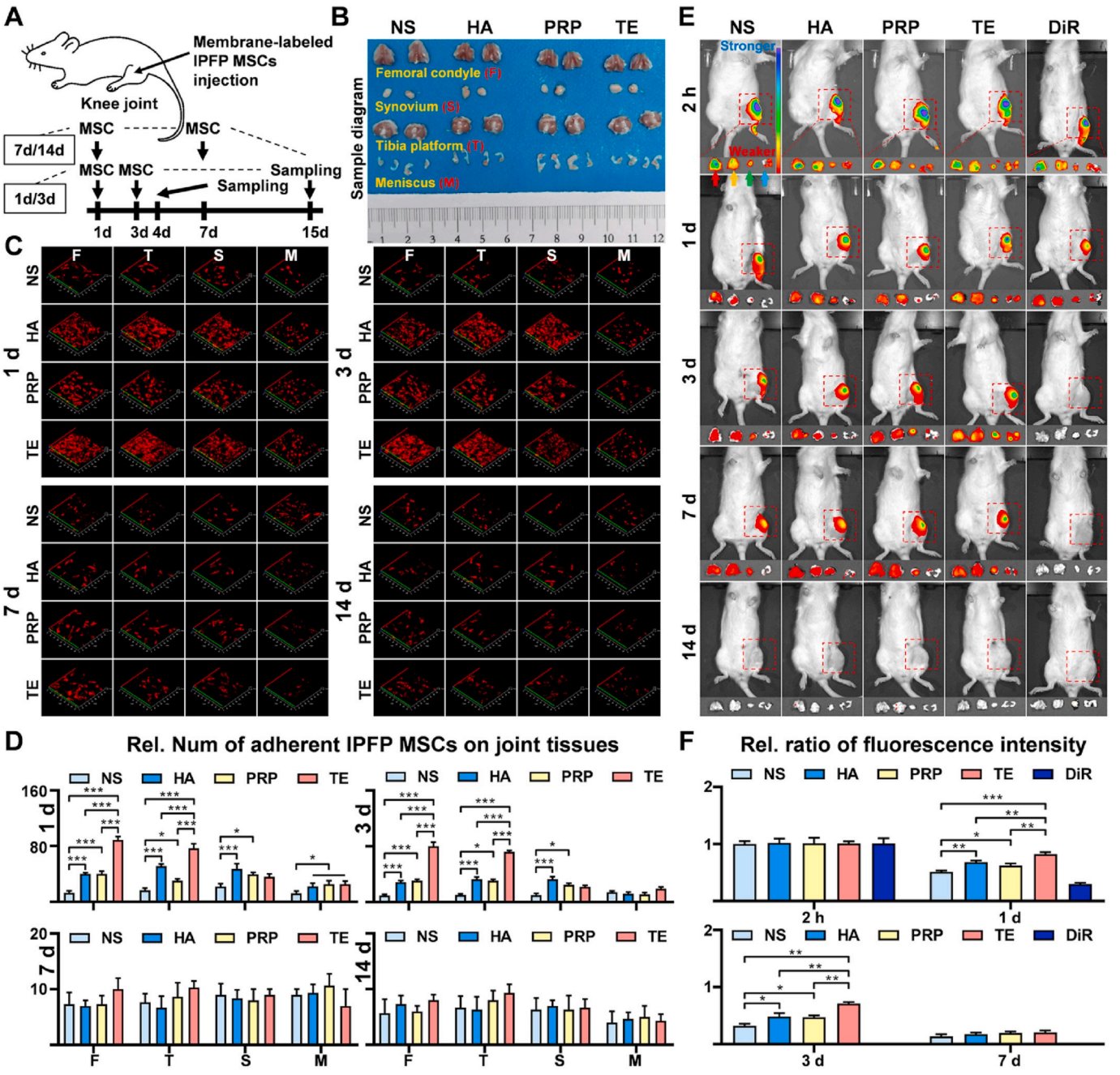

Fig. 6. TE promotes IPFP-MSCs survival and adhesion in SD rat joint cavity. (A) A flow diagram showing the labeled IPFP-MSCs and time of intra-articular injection (only one injection). (B) Sample diagram of rat knee joint (femoral condyle, tibia platform, synovium, and meniscus). (C) Fluorescence labeling of IPFP-MSCs attached to tissues (femoral condyle, tibia platform, synovium, and meniscus) in rat knee joint. (D) Quantitative analysis of IPFP-MSCs adhesion on rat femoral condyle or tibia platform or synovium or meniscus. (n = 6, *P < 0.05, ***P < 0.001). (E) Representative fluorescent *in vivo* image of OA rat knee joints over 14 days after intra-articular injection of DiR-IPFP-MSCs. Red, Yellow, green or blue arrows indicate femoral condyle, tibia platform, synovium or meniscus respectively. Rainbow color scale (Min: 1e5; Max: 1e6). (F) Quantitative analysis of area based on fluorescence intensity profiles (fluorescent *in vivo* imaging). (n = 6, *P < 0.05, **P < 0.01, ***P < 0.001).

The OARSI scoring was used to quantify the severity of cartilage damage, and the results revealed that TE, HA and PRP significantly reversed the cartilage lesion after ACLT surgery compared with NS. In the statistical analysis of relative staining intensity, ACLT group was weaker compared with NS, TE, HA, and PRP group, and TE, HA, and PRP group showed stronger intensity than NS group (Fig. 7F).

3.10. IPFP-MSCs pretreated with anti-integrin β1 or SCH772984 in TE solution cannot promote IPFP-MSCs survival-adhesion and demolishes remedial effect of TE-IPFP-MSC suspension on rat knee OA

To investigate whether integrin β1 or ERK1/2 was involved in TE-IPFP-MSCs suspension-mediated cartilage protection *in vivo*, we further used integrin β1 monoclonal antibody (anti-integrin β1) and ERK inhibitor (SCH772984) in ACLT rat model (Fig. 8A). IPFP-MSCs with or without pretreatment of anti-integrin β1 and SCH772984 were respectively injected into the knee joint of rats. Fluorescent *in vivo* imaging

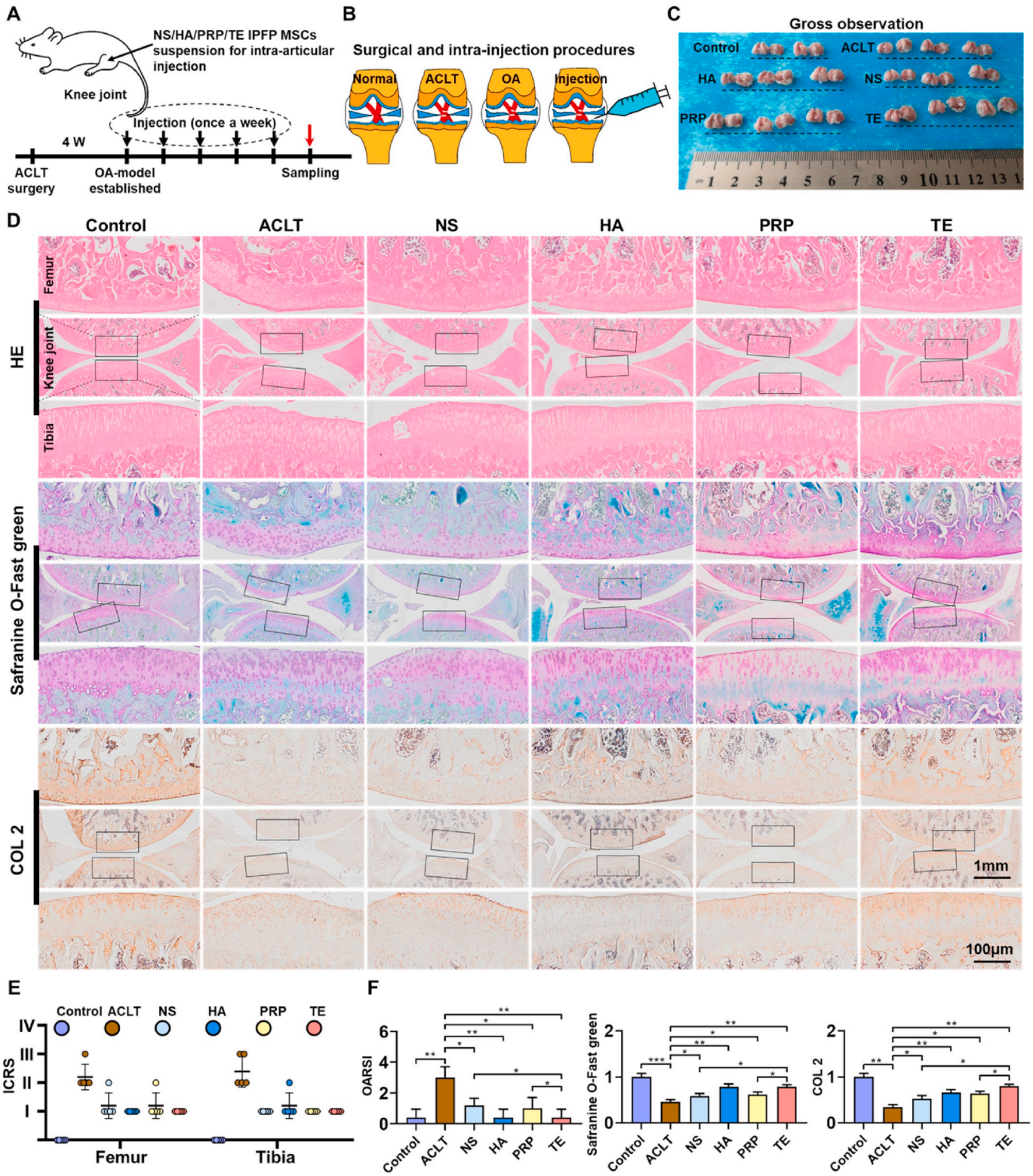

Fig. 7. Intra-articular injection of TE-IPFP-MSCs suspension reduces rat knee OA. (A) and (B) Schematic showing the surgical and intra-articular injection protocol of OA rat with ACLT surgery. Black arrows indicate time points when intra-articular injection was performed; red arrows indicate sampling time. (C) Macroscopic appearance of cartilage from femoral condyle and tibial plateaus of rats. (D) HE, safranin O-Fast Green, and COL 2 immunohistochemistry staining of rat knee joints. Images of femur and tibia are from black boxed area. (E) The ICRS scores for macroscopic observation of rat knee joints. (F) OARSI score (HE) and relative staining intensity (safranin O-Fast Green and COL 2 immunohistochemistry staining). (n = 8, *P < 0.05, **P < 0.01, ***P < 0.001).

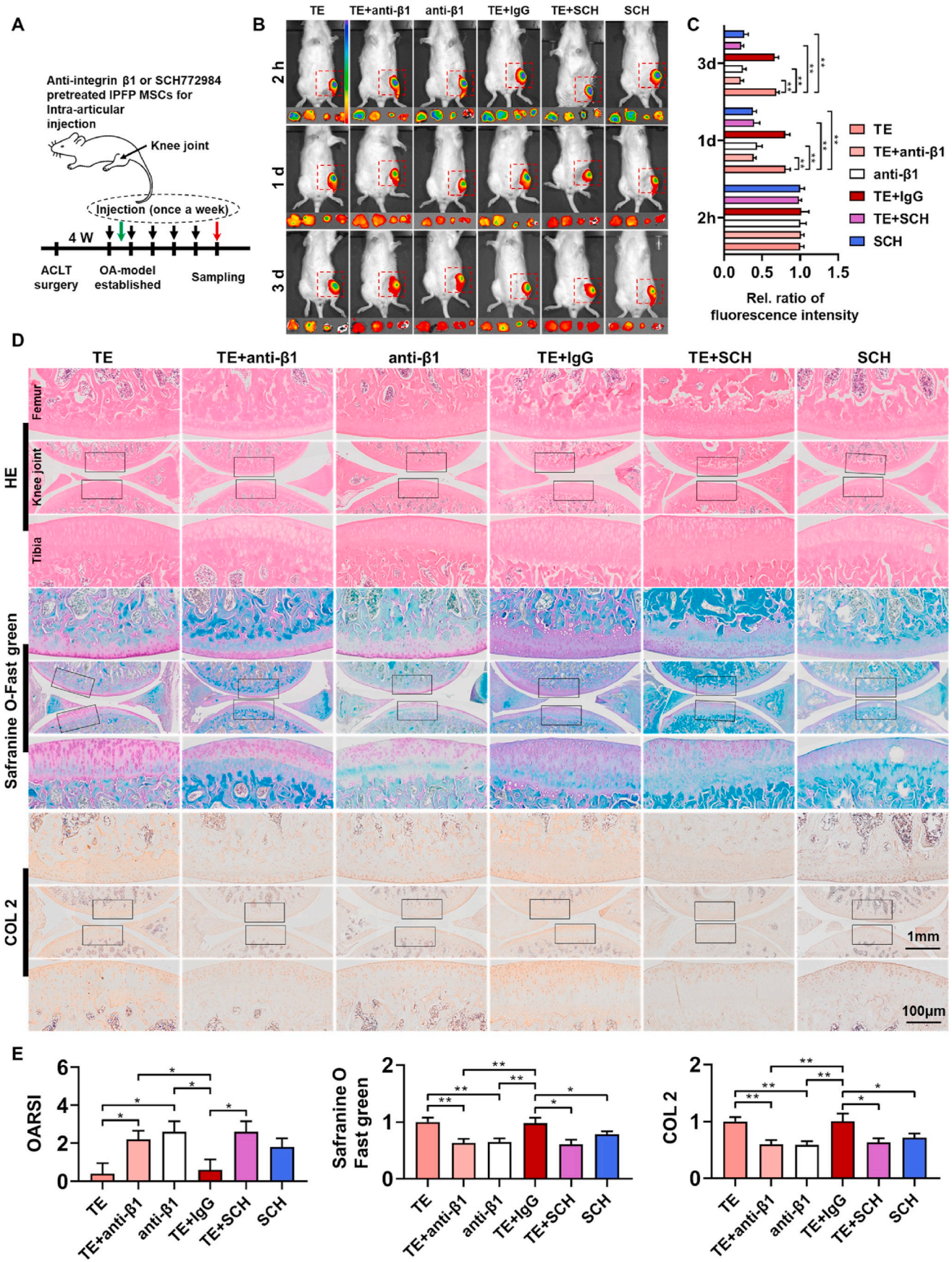

(caption on next page)

Fig. 8. Intra-articular injection of anti-integrin β1 or SCH772984 pretreated-IPFP-MSCs demolishes its survival and remedial effect of TE-IPFP-MSC suspension in ACLT rat model. (A) Schematic showing the intra-articular injection protocol of OA rat with ACLT surgery. Black arrows indicate time points when intra-articular injection was performed; green or red arrows indicates *in vivo* fluorescence imaging or histological sampling time. (B) Representative fluorescent *in vivo* image of OA rat knee joints over 3 days after intra-articular injection of anti-integrin β1 or SCH772984 pretreated DiR-IPFP MSCs. Rainbow color scale (Min: 1e5; Max: 1e6). (C) Quantitative analysis of area based on fluorescence intensity profiles (fluorescent *in vivo* imaging). (n = 6, **P < 0.01). (D) HE, safranin O-Fast Green, and COL 2 immunohistochemistry staining of rat knee joints. Images of femur and tibia were from black boxed area. (E) OARSI score (HE) and relative staining intensity (safranin O-Fast Green and COL 2 immunohistochemistry staining). (n = 6, *P < 0.05, **P < 0.01).

results (Fig. 8B and C) showed that fluorescence intensity of the TE + anti-β1, anti-β1, TE + SCH, and SCH group in rat knee joint was weaker than that in TE and TE + IgG group at 1 days or 3 days. In addition, HE and Safranin O/fast green staining showed that intra-articular injection of IPFP-MSCs pretreated with anti-integrin β1 or SCH772984 remarkably reduced effect of TE-IPFP-MSC suspension-mediated cartilage protection in ACLT-induced OA rats (Fig. 8D and E). Moreover, there was a decreased expression of collagen II in anti-integrin β1 and SCH772984 groups, as compared to TE group.

4. Discussion

Despite impressive potential of MSCs intra-articular injection therapy in OA treatment, several obstacles such as decrease of maintaining self-renewal ability, poor survival due to apoptosis, and difficulty of migrating to damage location remain [44–46]. Therefore, to efficiently maintain performance of MSCs is of significant clinical interest and could promote therapeutic effect on OA. Here we reported that TE not only markedly promoted adhesion, migration, chondrogenic differentiation, and paracrine function of IPFP MSCs, but also paralleled or surpassed performance of classical MSC-injection medium such as NS, HA, and PRP (Fig. S3J).

In this study, we chose human IPFP-MSCs as seeded cells because it is relative feasible to obtain IPFP from knee OA patients by arthroscopic operation in clinics. Besides, it has been shown that IPFP MSCs have a higher capacity for chondrogenic differentiation than MSCs from body fat, bone marrow, and umbilical cord [47]. Moreover, our group previously found that IPFP-MSCs combined with chitosan/hyaluronic acid nanoparticles promoted chondrogenic differentiation [48]; IPFP-MSC-derived exosomes protect cartilage from damage and ameliorate gait patterns of DMM-induced OA mice through inhibiting chondrocyte apoptosis and balancing anabolic-catabolic processes [31]. Therefore, we confirmed that IPFP-MSCs would have great potential for OA intra-articular injection.

When MSCs are injected into articular cavity, they encounter nutrient-oxygen deprivation environment coupled with death signals due to the inadequate tensegrity structure between the cells and matrix. The lack of matrix support and adhesion to ECM is called anoikis [49]. Anoikis is a form of programmed cell death that occurs due to the loss of anchorage-dependent attachment to the ECM [50]. Therefore, enhancing the adhesion of the transplanted MSCs through inhibition of anoikis should improve efficacy of MSC intra-articular-injection clinical applications. Here, our results showed that compared with NS, HA, and PRP solution, IPFP-MSCs suspended in TE solution had strong adhesion at early stages. Previous studies normally analyzed number of adherent cells, with no further analysis of the adhesion morphology of MSCs [51,52]. In this study, adhesion area and height of IPFP-MSCs at 2 h were detected by SEM and Pro-film 3D scanning. We found that TE could increase adhesion area and reduce height of most IPFP-MSCs at early stage. This change indicated a better adhesion of IPFP-MSCs, since it has been shown that decrease in cell height and increase in adhesion area could improve cell adhesion [53–56]. Besides, in order to simulate adhesion process of MSCs in the joint cavity, osteochondral composites were used for cartilage adhesion assay. Similarly, Baboolal et al. had used this method to study the synovial fluid hyaluronan mediated MSCs attachment to cartilage [32]. Consistent with data from IPFP MSCs adhesion on cell slides, TE also had a positive impact on IPFP-MSC-cartilage-adhesion *in vitro*.

To play the therapeutic role in knee OA, exogenous injected-MSCs should adhere to tissue in joint cavity at first and then migrate to inflammation-defect site [57]. The phenomenon that MSCs have the characteristics of dominant distribution to the injury site is called MSCs-homing. Previous studies have suggested HA-coatings as a simple approach to improve MSCs homing [58]; HA has been shown to induce MSCs migration and MSCs homing to injured tissue [59]. Here our results also showed that IPFP-MSCs in HA solution possessed better migration ability than that in NS. However, PRP was more effective than HA in promoting MSCs migration in our results, potentially due to the growth factors HGF, VEGF, PDGF, IGF, FGF, and CTGF contained in PRP [60,61]. It is worth mentioning that human PRP was injected into rat joint in our study. Human PRP or its biological products has been applied to rat disease-model before, which achieved good therapeutic effect and did not cause immune response [62–64]. This might be attributed to high homology in these chemokines-cytokines between human and rat. Interestingly, we found that TE promoted the migration of IPFP-MSCs both on cell slide and cartilage surface compared with NS, HA, and PRP. Consistent with our results, some previous studies have shown that TE promotes cell migration in other cell types. For example, 80% TE-20% collagen composite scaffold enhances fibroblast proliferation and migration [65]; magnetically responsive TE spongy-like hydrogels supported cell viability and enabled cell adhesion, spreading and migration into the interior of the spongy-like hydrogel [66]; TE stimulates endothelial cell migration and adhesion more than smooth muscle cells [67].

Then we further analyzed the VCL focal adhesion and cytoskeleton of IPFP-MSCs. Focal adhesions are large macromolecular assemblies which can transmit mechanical forces, regulate signals between ECM and interacting cells. Besides, VCL connects integrin to actomyosin networks and F-actin, providing a foundation for network formation within focal adhesions [68]. Our results revealed that TE can promote expression of VCL and cell spreading at the beginning of cell-adhesion. However, the cytoskeleton morphology and expression of VCL in IPFP-MSCs at 12 h showed no significant difference among three groups (HA, PRP, and TE).

Integrins are associated with cell-to-cell and cell-to ECM adhesion events via ECM binding and/or cell adhesion molecules [69]. To determine the involvement of integrin receptors in TE modulation of MSCs behavior, we analyzed the divalent cation dependence of TE-IPFP-MSCs interaction. Addition of the chelator EDTA significantly inhibited IPFP-MSCs attachment. Besides, gene levels of 10 integrins-subtypes and 16 adhesion related markers which are known to be expressed in ADSCs were measured [70]. In this study, expression of VCL, ERK, and integrin β1 was significantly increased in TE group. It has been reported that recombinant human transglutaminase 4 treatment induces expression of integrin β1 and dynamic actin fiber, enhancing synovium-derived MSCs adhesion to fibronectin [71]; BMSCs cultured on nanoparticle Titanium surface have more expression of integrin β1 and better adhesion [72]; periostin overexpression effectively enhances the migration and adhesion of ADSCs through integrin β1/FAK/Akt/-PI3K/eNOS signaling pathway [73]. Moreover, it has been shown that miRNA-125b can also promote the adhesion of suspended MSCs and resist anoikis by enhancing phosphorylation of ERK [74]; overexpression of integrin-linked kinase in MSCs could increase phosphorylation-ratio of ERK, which improves their adhesion and survival in joint [75,76]; activation of ERK pathway can promote MSCs-homing, which is expected to enhance potential of MSCs transplantation therapy [77,78]. Therefore, we assumed that TE took effects

through integrin β1/ERK/VCL pathway. To confirm the role of integrin β1/ERK in MSCs interactions with TE, specific integrin-blocking antibody and ERK1/2 inhibitor were used. Indeed, they impeded MSCs adhesion and expression of VCL in TE solution. Taken together, these results supported the role of integrin β1/ERK/VCL in mediating MSCs adhesion in TE solution.

The regenerative mechanisms of intra-articular injected MSCs in OA are not fully understood. Studies have suggested mechanisms including chondrogenic differentiation [79,80] and paracrine effects [81,82]. Here we assumed that activation of integrin β1/ERK/VCL pathway with treatment of TE solution improved the paracrine action of IPFP-MSCs, since enhancement of MSC adhesion could prevent its functional impairment and promote its paracrine therapeutic effect [83–85]. Besides, it has been shown that TE production is temporally and spatially linked to expression of type II collagen and proteoglycans [86], which is also beneficial for chondrogenesis. Note that HA also showed promising results in our study, which is in agreement with previous studies: MSCs with high density in HA hydrogels produce engineered cartilage with native tissue properties [87]; addition of HA improves cellular infiltration and promotes early-stage chondrogenesis in a collagen-based scaffold for cartilage tissue engineering [88]. However, IPFP-MSCs had less expression of chondrogenic markers in PRP group. We presumed that PRP could promote the osteogenic differentiation of MSCs as some studies have shown [89,90].

In the process of intra-articular injection therapy evaluation, tracing injected MSC inside host joint is considered essential. In our research, for tracking survival, distribution and adhesion of IPFP-MSCs *in vivo*, DiO, DiI, and DiR were used to label cells. At 1 d and 3 d, decrease of cell quantity in NS and PRP group was already detected in our OA rat models, while TE and HA solution could maintain adhesion of IPFP-MSCs to tissues in the joint. However, at 7 d and 14 d, four groups of IPFP-MSCs were almost “disappeared” in rat knee. We speculated that these injection solvents were gradually degraded and absorbed due to large amounts of degrading enzyme and inflammatory factors in OA knee joint such as matrix metalloproteinases (MMPs), hyaluronidase, and tissue inhibitor of metalloproteinases (TIMPs) [91–93]. Therefore, materials with controlled release of ECM proteins to protect MSCs-survival need further study.

Finally, the curative effect of IPFP-MSCs suspension on ACLT-induced OA was analyzed. Although there was no significant difference among four groups in gross observation, histological analysis suggested that TE-IPFP-MSCs solution effectively delayed rat OA progression compared with NS, HA, and PRP group; while anti-integrin β1 or SCH772984 preconditioned-IPFP-MSCs in TE solution had poor survival in joint and could not relieve OA aggravation. Therefore, it is suggested that the regulation of TE in IPFP-MSCs survival *in vivo* could also be related to integrin β1/ERK pathway [94,95].

5. Conclusion

Our study demonstrates that TE could promote performance of IPFP-MSCs, and protect knee cartilage from damage in ACLT-induced OA rats. The mechanism of TE regulating IPFP-MSCs adhesion *in vitro* and *in vivo* could be related to integrin β1/ERK/VCL pathway. As it is relatively convenient and feasible to apply TE as MSCs-injection-solvent in clinics, our findings may provide a new strategy for MSC intra-articular injection.

Funding

This work was supported by CHONGQING TALENTS PROJECT (4246ZJ1) and Science and technology projects of Chongqing Education Commission (KJQN202000427).

CRediT authorship contribution statement

Junjun Yang: Methodology, Investigation, Writing – original draft, Writing – review & editing. **Xin Wang:** Investigation. **Yahan Fan:** Conceptualization, Resources. **Xiongbo Song:** Investigation. **Jiangyi Wu:** Formal analysis. **Zhenlan Fu:** Investigation. **Tao Li:** Investigation. **Yang Huang:** Methodology, Investigation. **ZheXiong Tang:** Investigation. **Shuo Meng:** Investigation. **Na Liu:** Investigation. **Jiajia Chen:** Investigation. **Pingju Liu:** Investigation. **Liu Yang:** Conceptualization, Funding acquisition. **Xiaoyuan Gong:** Conceptualization, Writing – original draft. **Cheng Chen:** Conceptualization, Writing – original draft, Writing – review & editing, Supervision, Funding acquisition.

Declaration of competing interest

The authors declare no conflicts of interest.

Acknowledgement

We thank Prof. Guangxing Chen, Dr. Dejie Fu, and Dr. Ran Xiong for helpful suggestions. We thank the technical support in histologic staining offered by Knorigene Technologies. We thank Kunming Baker Norton Pharmaceutical for donating Hyaluronic acid (HA, ARTZ® Dispo, Imported Drug License: H20140533) for our research.

Appendix A. Supplementary data

Supplementary data to this article can be found online at https://doi.org/10.1016/j.bioactmat.2021.09.011.

References

[1] X.D. Wu, D. Wu, W. Huang, G.X. Qiu, Relation between cartilage loss and pain in knee osteoarthritis, Ann. Rheum. Dis. (2020 Oct 7) annrheumdis-2020-218433.
[2] J.J. Hwang, Y.A. Rim, Y. Nam, J.H. Ju, Recent developments in clinical applications of mesenchymal stem cells in the treatment of rheumatoid arthritis and osteoarthritis, Front. Immunol. 12 (2021), 631291.
[3] R. Zhang, J. Ma, J. Han, W. Zhang, J. Ma, Mesenchymal stem cell related therapies for cartilage lesions and osteoarthritis, Am. J. Tourism Res. 11 (10) (2019) 6275–6289.
[4] R. Bastos, M. Mathias, R. Andrade, R. Amaral, V. Schott, A. Balduino, R. Bastos, J. Miguel Oliveira, R.L. Reis, S. Rodeo, J. Espregueira-Mendes, Intra-articular injection of culture-expanded mesenchymal stem cells with or without addition of platelet-rich plasma is effective in decreasing pain and symptoms in knee osteoarthritis: A controlled, double-blind clinical trial, Knee surgery, sports traumatology, arthroscopy, Official J. ESSKA 28 (6) (2020) 1989–1999.
[5] M. Emadedin, N. Labibzadeh, M.G. Liastani, A. Karimi, N. Jaroughi, T. Bolurieh, S. E. Hosseini, H. Baharvand, N. Aghdami, Intra-articular implantation of autologous bone marrow-derived mesenchymal stromal cells to treat knee osteoarthritis: a randomized, triple-blind, placebo-controlled phase 1/2 clinical trial, Cytotherapy 20 (10) (2018) 1238–1246.
[6] J. Higuchi, R. Yamagami, T. Matsumoto, T. Terao, K. Inoue, S. Tsuji, Y. Maenohara, T. Matsuzaki, R. Chijimatsu, Y. Omata, F. Yano, S. Tanaka, T. Saito, Associations of clinical outcomes and MRI findings in intra-articular administration of autologous adipose-derived stem cells for knee osteoarthritis, Regenerative Therapy 14 (2020) 332–340.
[7] W. Tong, X. Zhang, Q. Zhang, J. Fang, Y. Liu, Z. Shao, S. Yang, D. Wu, X. Sheng, Y. Zhang, H. Tian, Multiple umbilical cord-derived MSCs administrations attenuate rat osteoarthritis progression via preserving articular cartilage superficial layer cells and inhibiting synovitis, J. Orthopaedic. Translation 23 (2020) 21–28.
[8] Y. Hu, H. Wu, T. Xu, Y. Wang, H. Qin, Z. Yao, P. Chen, Y. Xie, Z. Ji, K. Yang, Y. Chai, X. Zhang, B. Yu, Z. Cui, Defactinib attenuates osteoarthritis by inhibiting positive feedback loop between H-type vessels and MSCs in subchondral bone, J. Orthopaedic Translation 24 (2020) 12–22.
[9] W. Dai, X. Leng, J. Wang, Z. Shi, J. Cheng, X. Hu, Y. Ao, Intra-articular mesenchymal stromal cell injections are No different from placebo in the treatment of knee osteoarthritis: a systematic review and meta-analysis of randomized controlled trials, Arthroscopy.: J. Arthroscopic. Related Surgery.: Official Publication Arthroscopy Association North Am. Int. Arthroscopy Assoc. 37 (1) (2021) 340–358.
[10] T. Xia, F. Yu, K. Zhang, Z. Wu, D. Shi, H. Teng, J. Shen, X. Yang, Q. Jiang, The effectiveness of allogeneic mesenchymal stem cells therapy for knee osteoarthritis in pigs, Ann. Transl. Med. 6 (20) (2018) 404.
[11] H.L. Reesink, R.M. Sutton, C.R. Shurer, R.P. Peterson, J.S. Tan, J. Su, M.J. Paszek, A.J. Nixon, Galectin-1 and galectin-3 expression in equine mesenchymal stromal

cells (MSCs), synovial fibroblasts and chondrocytes, and the effect of inflammation on MSC motility, Stem Cell Res. Ther. 8 (1) (2017) 243.
[12] X.H. Jing, L. Yang, X.J. Duan, B. Xie, W. Chen, Z. Li, H.B. Tan, In vivo MR imaging tracking of magnetic iron oxide nanoparticle labeled, engineered, autologous bone marrow mesenchymal stem cells following intra-articular injection, Joint Bone Spine 75 (4) (2008) 432–438.
[13] J.A. McIntyre, I.A. Jones, B. Han, C.T. Vangsness Jr., Intra-articular mesenchymal stem cell therapy for the human joint: A systematic review, Am. J. Sports Med. 46 (14) (2018) 3550–3563.
[14] X. Zhang, J. He, W. Wang, Progress in the use of mesenchymal stromal cells for osteoarthritis treatment, Cytotherapy 23 (6) (2021) 459–470.
[15] C. Kim, A. Keating, Cell therapy for knee osteoarthritis: mesenchymal stromal cells, Gerontology 65 (3) (2019) 294–298.
[16] F. Barry, MSC therapy for osteoarthritis: an unfinished story, J. Orthop. Res.; Official Publication Orthopaedic Res. Soc. 37 (6) (2019) 1229–1235.
[17] M. ter Huurne, R. Schelbergen, R. Blattes, A. Blom, W. de Munter, L.C. Grevers, J. Jeanson, D. Noël, L. Casteilla, C. Jorgensen, W. van den Berg, P.L. van Lent, Antiinflammatory and chondroprotective effects of intraarticular injection of adipose-derived stem cells in experimental osteoarthritis, Arthritis Rheum. 64 (11) (2012) 3604–3613.
[18] G.M. van Buul, M. Siebelt, M.J. Leijs, P.K. Bos, J.H. Waarsing, N. Kops, H. Weinans, J.A. Verhaar, M.R. Bernsen, G.J. van Osch, Mesenchymal stem cells reduce pain but not degenerative changes in a mono-iodoacetate rat model of osteoarthritis, J. Orthop. Res. : Official Publication Orthopaedic Res. Soc. 32 (9) (2014) 1167–1174.
[19] M. Emadedin, N. Aghdami, L. Taghiyar, R. Fazeli, R. Moghadasali, S. Jahangir, R. Farjad, M. Baghaban Eslaminejad, Intra-articular injection of autologous mesenchymal stem cells in six patients with knee osteoarthritis, Arch. Iran. Med. 15 (7) (2012) 422–428.
[20] J.M. Murphy, D.J. Fink, E.B. Hunziker, F.P. Barry, Stem cell therapy in a caprine model of osteoarthritis, Arthritis Rheum. 48 (12) (2003) 3464–3474.
[21] J. Mak, C.L. Jablonski, C.A. Leonard, J.F. Dunn, E. Raharjo, J.R. Matyas, J. Biernaskie, R.J. Krawetz, Intra-articular injection of synovial mesenchymal stem cells improves cartilage repair in a mouse injury model, Sci. Rep. 6 (2016) 23076.
[22] B.O. Diekman, C.L. Wu, C.R. Louer, B.D. Furman, J.L. Huebner, V.B. Kraus, S. A. Olson, F. Guilak, Intra-articular delivery of purified mesenchymal stem cells from C57BL/6 or MRL/MpJ superhealer mice prevents posttraumatic arthritis, Cell Transplant. 22 (8) (2013) 1395–1408.
[23] S. Lee, E. Choi, M.J. Cha, K.C. Hwang, Cell adhesion and long-term survival of transplanted mesenchymal stem cells: a prerequisite for cell therapy, 2015, Oxidative Med. Cellular Longevity (2015), 632902.
[24] S.G. Wise, A.S. Weiss, Tropoelastin, The Int. J. Biochem. Cell Biol. 41 (3) (2009) 494–497.
[25] P. Lee, G.C. Yeo, A.S. Weiss, A cell adhesive peptide from tropoelastin promotes sequential cell attachment and spreading via distinct receptors, FEBS J. 284 (14) (2017) 2216–2230.
[26] D.V. Bax, A. Kondyurin, A. Waterhouse, D.R. McKenzie, A.S. Weiss, M.M. Bilek, Surface plasma modification and tropoelastin coating of a polyurethane co-polymer for enhanced cell attachment and reduced thrombogenicity, Biomaterials 35 (25) (2014) 6797–6809.
[27] G.C. Yeo, A.S. Weiss, Soluble matrix protein is a potent modulator of mesenchymal stem cell performance, Proc. Natl. Acad. Sci. U. S. A. 116 (6) (2019) 2042–2051.
[28] P. Neybecker, C. Henrionnet, E. Pape, D. Mainard, L. Galois, D. Loeuille, P. Gillet, A. Pinzano, In vitro and in vivo potentialities for cartilage repair from human advanced knee osteoarthritis synovial fluid-derived mesenchymal stem cells, Stem Cell Res. Ther. 9 (1) (2018) 329.
[29] L. Li, X. Duan, Z. Fan, L. Chen, F. Xing, Z. Xu, Q. Chen, Z. Xiang, Mesenchymal stem cells in combination with hyaluronic acid for articular cartilage defects, Sci. Rep. 8 (1) (2018) 9900.
[30] Y.G. Koh, Y.J. Choi, Infrapatellar fat pad-derived mesenchymal stem cell therapy for knee osteoarthritis, Knee 19 (6) (2012) 902–907.
[31] J. Wu, L. Kuang, C. Chen, J. Yang, W.N. Zeng, T. Li, H. Chen, S. Huang, Z. Fu, J. Li, R. Liu, Z. Ni, L. Chen, L. Yang, miR-100-5p-abundant exosomes derived from infrapatellar fat pad MSCs protect articular cartilage and ameliorate gait abnormalities via inhibition of mTOR in osteoarthritis, Biomaterials 206 (2019) 87–100.
[32] T.G. Baboolal, S.C. Mastbergen, E. Jones, S.J. Calder, F.P. Lafeber, D. McGonagle, Synovial fluid hyaluronan mediates MSC attachment to cartilage, a potential novel mechanism contributing to cartilage repair in osteoarthritis using knee joint distraction, Ann. Rheum. Dis. 75 (5) (2016) 908–915.
[33] B.N. Dittel, J.B. McCarthy, E.A. Wayner, T.W. LeBien, Regulation of human B-cell precursor adhesion to bone marrow stromal cells by cytokines that exert opposing effects on the expression of vascular cell adhesion molecule-1 (VCAM-1), Blood 81 (9) (1993) 2272–2282.
[34] Y. Yokosaki, E.L. Palmer, A.L. Prieto, K.L. Crossin, M.A. Bourdon, R. Pytela, D. Sheppard, The integrin alpha 9 beta 1 mediates cell attachment to a non-RGD site in the third fibronectin type III repeat of tenascin, J. Biol. Chem. 269 (43) (1994) 26691–26696.
[35] Q. Wang, B. Shen, L. Chen, P. Zheng, H. Feng, Q. Hao, X. Liu, L. Liu, S. Xu, J. Chen, J. Teng, Extracellular calumenin suppresses ERK1/2 signaling and cell migration by protecting fibulin-1 from MMP-13-mediated proteolysis, Oncogene 34 (8) (2015) 1006–1018.
[36] E.J. Morris, S. Jha, C.R. Restaino, P. Dayananth, H. Zhu, A. Cooper, D. Carr, Y. Deng, W. Jin, S. Black, B. Long, J. Liu, E. Dinunzio, W. Windsor, R. Zhang, S. Zhao, M.H. Angagaw, E.M. Pinheiro, J. Desai, L. Xiao, G. Shipps, A. Hruza, J. Wang, J. Kelly, S. Paliwal, X. Gao, B.S. Babu, L. Zhu, P. Daublain, L. Zhang, B. A. Lutterbach, M.R. Pelletier, U. Philippar, P. Siliphaivanh, D. Witter, P. Kirschmeier, W.R. Bishop, D. Hicklin, D.G. Gilliland, L. Jayaraman, L. Zawel, S. Fawell, A.A. Samatar, Discovery of a novel ERK inhibitor with activity in models of acquired resistance to BRAF and MEK inhibitors, Canc. Discov. 3 (7) (2013) 742–750.
[37] S. Luo, Q. Shi, W. Li, W. Wu, Z. Zha, ITGB1 promotes the chondrogenic differentiation of human adipose-derived mesenchymal stem cells by activating the ERK signaling, J. Mol. Histol. 51 (6) (2020) 729–739.
[38] N. Liu, D. Fu, J. Yang, P. Liu, X. Song, X. Wang, R. Li, Z. Fu, J. Chen, X. Gong, C. Chen, L. Yang, Asiatic acid attenuates hypertrophic and fibrotic differentiation of articular chondrocytes via AMPK/PI3K/AKT signaling pathway, Arthritis Res. Ther. 22 (1) (2020) 112.
[39] N. Gerwin, A.M. Bendele, S. Glasson, C.S. Carlson, The OARSI histopathology initiative - recommendations for histological assessments of osteoarthritis in the rat, Osteoarthritis Cartilage 18 (3) (2010) S24–S34.
[40] Z. Fu, X. Song, L. Guo, L. Yang, C. Chen, Effects of conditioned medium from osteoarthritic cartilage fragments on donor-matched infrapatellar fat pad-derived mesenchymal stromal cells, Am. J. Sports Med. 47 (12) (2019) 2927–2936.
[41] M. Dominici, K. Le Blanc, I. Mueller, I. Slaper-Cortenbach, F. Marini, D. Krause, R. Deans, A. Keating, D. Prockop, E. Horwitz, Minimal criteria for defining multipotent mesenchymal stromal cells, Int. Soc. Cellular Therapy Position Statement, Cytotherapy 8 (4) (2006) 315–317.
[42] J. Yang, X. Song, Y. Feng, N. Liu, Z. Fu, J. Wu, T. Li, H. Chen, J. Chen, C. Chen, L. Yang, Natural ingredients-derived antioxidants attenuate H(2)O(2)-induced oxidative stress and have chondroprotective effects on human osteoarthritic chondrocytes via Keap1/Nrf2 pathway, Free Radical Biol. Med. 152 (2020) 854–864.
[43] D.S. Chae, C.Y. Lee, J. Lee, H.H. Seo, C.H. Choi, S. Lee, K.C. Hwang, Priming stem cells with protein kinase C activator enhances early stem cell-chondrocyte interaction by increasing adhesion molecules, Biol. Res. 51 (1) (2018) 41.
[44] A. Colombini, C. Perucca Orfei, D. Kouroupis, E. Ragni, P. De Luca, M. ViganÒ, D. Correa, L. de Girolamo, Mesenchymal stem cells in the treatment of articular cartilage degeneration: new biological insights for an old-timer cell, Cytotherapy 21 (12) (2019) 1179–1197.
[45] M. Ruiz, S. Cosenza, M. Maumus, C. Jorgensen, D. Noël, Therapeutic application of mesenchymal stem cells in osteoarthritis, Expet Opin. Biol. Ther. 16 (1) (2016) 33–42.
[46] M.K. Mamidi, A.K. Das, Z. Zakaria, R. Bhonde, Mesenchymal stromal cells for cartilage repair in osteoarthritis, Osteoarthritis Cartilage 24 (8) (2016) 1307–1316.
[47] D.C. Ding, K.C. Wu, H.L. Chou, W.T. Hung, H.W. Liu, T.Y. Chu, Human infrapatellar fat pad-derived stromal cells have more potent differentiation capacity than other mesenchymal cells and can Be enhanced by hyaluronan, Cell Transplant. 24 (7) (2015) 1221–1232.
[48] S. Huang, X. Song, T. Li, J. Xiao, Y. Chen, X. Gong, W. Zeng, L. Yang, C. Chen, Pellet coculture of osteoarthritic chondrocytes and infrapatellar fat pad-derived mesenchymal stem cells with chitosan/hyaluronic acid nanoparticles promotes chondrogenic differentiation, Stem Cell Res. Ther. 8 (1) (2017) 264.
[49] J.R.W. Conway, G. Jacquemet, Cell matrix adhesion in cell migration, Essays Biochem. 63 (5) (2019) 535–551.
[50] J.B. Michel, Anoikis in the cardiovascular system: known and unknown extracellular mediators, Arterioscler. Thromb. Vasc. Biol. 23 (12) (2003) 2146–2154.
[51] W. Li, H. Xu, X. Han, S. Sun, Q. Chai, X. Xu, Z. Man, Simultaneously promoting adhesion and osteogenic differentiation of bone marrow-derived mesenchymal cells by a functional electrospun scaffold, Colloids Surf. B Biointerfaces 192 (2020), 111040.
[52] J.M. Sierra-Parraga, A. Merino, M. Eijken, H. Leuvenink, R. Ploeg, B.K. Møller, B. Jespersen, C.C. Baan, M.J. Hoogduijn, Reparative effect of mesenchymal stromal cells on endothelial cells after hypoxic and inflammatory injury, Stem Cell Res. Ther. 11 (1) (2020) 352.
[53] S. Wang, J. Wang, T. Ju, F. Yang, K. Qu, W. Liu, Z. Wang, Study of NSCLC cell migration promoted by NSCLC-derived extracellular vesicle using atomic force microscopy, Analytical methods : advancing methods and applications 13 (12) (2021) 1455–1462.
[54] A. Makowiecka, E. Mazurkiewicz, E. Mrówczyńska, N. Malek, A. Battistella, M. Lazzarino, D. Nowak, A.J. Mazur, Changes in biomechanical properties of A375 cells due to the silencing of TMSB4X expression are not directly correlated with alterations in their stemness features, Cells 10 (4) (2021).
[55] J.A. Castillo-Badillo, N. Gautam, An optogenetic model reveals cell shape regulation through FAK and fascin, J. Cell Sci. 134 (13) (2021).
[56] A.S. Ribeiro, F.A. Carvalho, J. Figueiredo, R. Carvalho, T. Mestre, J. Monteiro, A. F. Guedes, M. Fonseca, J. Sanches, R. Seruca, N.C. Santos, J. Paredes, Atomic force microscopy and graph analysis to study the P-cadherin/SFK mechanotransduction signalling in breast cancer cells, Nanoscale 8 (46) (2016) 19390–19401.
[57] O.I. Eseonu, C. De Bari, Homing of mesenchymal stem cells: mechanistic or stochastic? Implications for targeted delivery in arthritis, Rheumatology 54 (2) (2015) 210–218.
[58] B. Corradetti, F. Taraballi, J.O. Martinez, S. Minardi, N. Basu, G. Bauza, M. Evangelopoulos, S. Powell, C. Corbo, E. Tasciotti, Hyaluronic acid coatings as a simple and efficient approach to improve MSC homing toward the site of inflammation, Sci. Rep. 7 (1) (2017) 7991.
[59] X.H. Bian, G.Y. Zhou, L.N. Wang, J.F. Ma, Q.L. Fan, N. Liu, Y. Bai, W. Guo, Y. Q. Wang, G.P. Sun, P. He, X. Yang, X.S. Su, F. Du, G.F. Zhao, J.N. Miao, L. Ma, L. Q. Zheng, D.T. Li, J.M. Feng, The role of CD44-hyaluronic acid interaction in exogenous mesenchymal stem cells homing to rat remnant kidney, Kidney Blood Press. Res. 38 (1) (2013) 11–20.

[60] N. Araya, K. Miyatake, K. Tsuji, H. Katagiri, Y. Nakagawa, T. Hoshino, H. Onuma, S. An, H. Nishio, Y. Saita, I. Sekiya, H. Koga, Intra-articular injection of pure platelet-rich plasma is the most effective treatment for joint pain by modulating synovial inflammation and calcitonin gene-related peptide expression in a rat arthritis model, Am. J. Sports Med. 48 (8) (2020) 2004–2012.
[61] C.G. Ziegler, R. Van Sloun, S. Gonzalez, K.E. Whitney, N.N. DePhillipo, M. I. Kennedy, G.J. Dornan, T.A. Evans, J. Huard, R.F. LaPrade, Characterization of growth factors, cytokines, and chemokines in bone marrow concentrate and platelet-rich plasma: a prospective analysis, Am. J. Sports Med. 47 (9) (2019) 2174–2187.
[62] S.C. Tao, T. Yuan, B.Y. Rui, Z.Z. Zhu, S.C. Guo, C.Q. Zhang, Exosomes derived from human platelet-rich plasma prevent apoptosis induced by glucocorticoid-associated endoplasmic reticulum stress in rat osteonecrosis of the femoral head via the Akt/Bad/Bcl-2 signal pathway, Theranostics 7 (3) (2017) 733–750.
[63] M. Samberg, R. Stone 2nd, S. Natesan, A. Kowalczewski, S. Becerra, N. Wrice, A. Cap, R. Christy, Platelet rich plasma hydrogels promote in vitro and in vivo angiogenic potential of adipose-derived stem cells, Acta Biomater. 87 (2019) 76–87.
[64] S. Zhang, P. Li, Z. Yuan, J. Tan, Platelet-rich plasma improves therapeutic effects of menstrual blood-derived stromal cells in rat model of intrauterine adhesion, Stem Cell Res. Ther. 10 (1) (2019) 61.
[65] J. Rnjak-Kovacina, S.G. Wise, Z. Li, P.K. Maitz, C.J. Young, Y. Wang, A.S. Weiss, Electrospun synthetic human elastin:collagen composite scaffolds for dermal tissue engineering, Acta Biomater. 8 (10) (2012) 3714–3722.
[66] T. Pesqueira, R. Costa-Almeida, S.M. Mithieux, P.S. Babo, A.R. Franco, B. B. Mendes, R.M.A. Domingues, P. Freitas, R.L. Reis, M.E. Gomes, A.S. Weiss, Engineering magnetically responsive tropoelastin spongy-like hydrogels for soft tissue regeneration, J. Mater. Chem. B 6 (7) (2018) 1066–1075.
[67] B.D. Wilson, C.C. Gibson, L.K. Sorensen, M.Y. Guilhermier, M. Clinger, L.L. Kelley, Y.T. Shiu, D.Y. Li, Novel approach for endothelializing vascular devices: understanding and exploiting elastin-endothelial interactions, Ann. Biomed. Eng. 39 (1) (2011) 337–346.
[68] P.S. Mathieu, E.G. Loboa, Cytoskeletal and focal adhesion influences on mesenchymal stem cell shape, mechanical properties, and differentiation down osteogenic, adipogenic, and chondrogenic pathways, Tissue engineering, Part B, Reviews 18 (6) (2012) 436–444.
[69] F. Nitzsche, C. Müller, B. Lukomska, J. Jolkkonen, A. Deten, J. Boltze, Concise review: MSC adhesion cascade-insights into homing and transendothelial migration, Stem cells (Dayton, Ohio) 35 (6) (2017) 1446–1460.
[70] K.M. Yamada, B. Geiger, Molecular interactions in cell adhesion complexes, Curr. Opin. Cell Biol. 9 (1) (1997) 76–85.
[71] J.K. Kim, H.C. Bae, D.H. Ro, S. Lee, M.C. Lee, H.S. Han, Enhancement of cartilage regeneration of synovial stem cells/hydrogel by using transglutaminase-4, Tissue Eng. 27 (11–12) (2021 Jun) 761–770.
[72] L. Chen, J. Sun, Z. Zhu, K. Wu, W. Li, H. Liu, S. Xu, The adhesion and proliferation of bone marrow-derived mesenchymal stem cells promoted by nanoparticle surface, J. Biomater. Appl. 27 (5) (2013) 525–536.
[73] J. Qin, F. Yuan, Z. Peng, K. Ye, X. Yang, L. Huang, M. Jiang, X. Lu, Periostin enhances adipose-derived stem cell adhesion, migration, and therapeutic efficiency in Apo E deficient mice with hind limb ischemia, Stem Cell Res. Ther. 6 (1) (2015) 138.
[74] X. Yu, D.M. Cohen, C.S. Chen, miR-125b Is an adhesion-regulated microRNA that protects mesenchymal stem cells from anoikis, Stem cells (Dayton, Ohio) 30 (5) (2012) 956–964.
[75] D.S. Benoit, M.C. Tripodi, J.O. Blanchette, S.J. Langer, L.A. Leinwand, K.S. Anseth, Integrin-linked kinase production prevents anoikis in human mesenchymal stem cells, J. Biomed. Mater. Res. 81 (2) (2007) 259–268.
[76] S.W. Song, W. Chang, B.W. Song, H. Song, S. Lim, H.J. Kim, M.J. Cha, E. Choi, S. H. Im, B.C. Chang, N. Chung, Y. Jang, K.C. Hwang, Integrin-linked kinase is required in hypoxic mesenchymal stem cells for strengthening cell adhesion to ischemic myocardium, Stem cells (Dayton, Ohio) 27 (6) (2009) 1358–1365.
[77] M. Ishii, M. Takahashi, J. Murakami, T. Yanagisawa, M. Nishimura, Vascular endothelial growth factor-C promotes human mesenchymal stem cell migration via an ERK-and FAK-dependent mechanism, Mol. Cell. Biochem. 455 (1–2) (2019) 185–193.
[78] J. Alanko, A. Mai, G. Jacquemet, K. Schauer, R. Kaukonen, M. Saari, B. Goud, J. Ivaska, Integrin endosomal signalling suppresses anoikis, Nat. Cell Biol. 17 (11) (2015) 1412–1421.
[79] M. Shariatzadeh, J. Song, S.L. Wilson, The efficacy of different sources of mesenchymal stem cells for the treatment of knee osteoarthritis, Cell Tissue Res. 378 (3) (2019) 399–410.
[80] M. Zhou, N. Lozano, J.K. Wychowaniec, T. Hodgkinson, S.M. Richardson, K. Kostarelos, J.A. Hoyland, Graphene oxide: a growth factor delivery carrier to enhance chondrogenic differentiation of human mesenchymal stem cells in 3D hydrogels, Acta Biomater. 96 (2019) 271–280.
[81] Y.G. Kim, J. Choi, K. Kim, Mesenchymal stem cell-derived exosomes for effective cartilage tissue repair and treatment of osteoarthritis, Biotechnol. J. 15 (12) (2020), e2000082.
[82] Z. Ni, S. Zhou, S. Li, L. Kuang, H. Chen, X. Luo, J. Ouyang, M. He, X. Du, L. Chen, Exosomes: roles and therapeutic potential in osteoarthritis, Bone research 8 (2020) 25.
[83] Y.H. Cho, M.J. Cha, B.W. Song, I.K. Kim, H. Song, W. Chang, S. Lim, O. Ham, S. Y. Lee, E. Choi, H.M. Kwon, K.C. Hwang, Enhancement of MSC adhesion and therapeutic efficiency in ischemic heart using lentivirus delivery with periostin, Biomaterials 33 (5) (2012) 1376–1385.
[84] D.P. Kavanagh, J. Robinson, N. Kalia, Mesenchymal stem cell priming: fine-tuning adhesion and function, Stem cell reviews and reports 10 (4) (2014) 587–599.
[85] D. Chabot, A. Lewin, L. Loubaki, R. Bazin, Functional impairment of MSC induced by transient warming events: correlation with loss of adhesion and altered cell size, Cytotherapy 20 (8) (2018) 990–1000.
[86] K.A. Lee, R.A. Pierce, R.P. Mecham, W.C. Parks, Increased mesenchymal cell density accompanies induction of tropoelastin expression in developing elastic tissue, Dev. Dynam. : an official publication of the American Association of Anatomists 200 (1) (1994) 53–67.
[87] I.E. Erickson, S.R. Kestle, K.H. Zellars, M.J. Farrell, M. Kim, J.A. Burdick, R. L. Mauck, High mesenchymal stem cell seeding densities in hyaluronic acid hydrogels produce engineered cartilage with native tissue properties, Acta Biomater. 8 (8) (2012) 3027–3034.
[88] A. Matsiko, T.J. Levingstone, F.J. O'Brien, J.P. Gleeson, Addition of hyaluronic acid improves cellular infiltration and promotes early-stage chondrogenesis in a collagen-based scaffold for cartilage tissue engineering, Journal of the mechanical behavior of biomedical materials 11 (2012) 41–52.
[89] V. D'Esposito, M. Lecce, G. Marenzi, S. Cabaro, M.R. Ambrosio, G. Sammartino, S. Misso, T. Migliaccio, P. Liguoro, F. Oriente, L. Fortunato, F. Beguinot, J. C. Sammartino, P. Formisano, R. Gasparro, Platelet-rich plasma counteracts detrimental effect of high-glucose concentrations on mesenchymal stem cells from Bichat fat pad, Journal of tissue engineering and regenerative medicine 14 (5) (2020) 701–713.
[90] Y. Xie, M. Chen, Y. Chen, Y. Xu, Y. Sun, J. Liang, Y. Fan, X. Zhang, Effects of PRP and LyPRP on osteogenic differentiation of MSCs, J. Biomed. Mater. Res. 108 (1) (2020) 116–126.
[91] M.F. Hsueh, P. Önnerfjord, V.B. Kraus, Biomarkers and proteomic analysis of osteoarthritis, Matrix biology, journal of the International Society for Matrix Biology 39 (2014) 56–66.
[92] I. Tchetverikov, L.S. Lohmander, N. Verzijl, T.W. Huizinga, J.M. TeKoppele, R. Hanemaaijer, J. DeGroot, MMP protein and activity levels in synovial fluid from patients with joint injury, inflammatory arthritis, and osteoarthritis, Ann. Rheum. Dis. 64 (5) (2005) 694–698.
[93] M. Maiotti, G. Monteleone, U. Tarantino, G.F. Fasciglione, S. Marini, M. Coletta, Correlation between osteoarthritic cartilage damage and levels of proteinases and proteinase inhibitors in synovial fluid from the knee joint, Arthroscopy : The J. Arthroscopic Related Surgery : Official Publication Arthroscopy Assoc. North Am. Int. Arthroscopy Assoc. 16 (5) (2000) 522–526.
[94] J. Commins, R. Irwin, A. Matuska, M. Goodale, M. Delco, L. Fortier, Biological mechanisms for cartilage repair using a BioCartilage scaffold: cellular adhesion/migration and bioactive proteins, Cartilage (2020), 1947603519900803.
[95] Y.K. Wang, C.S. Chen, Cell adhesion and mechanical stimulation in the regulation of mesenchymal stem cell differentiation, J. Cell Mol. Med. 17 (7) (2013) 823–832.